Defence Research and Development Canada
Recherche et développement pour la défense Canada

DEFENCE R&D DÉFENSE

Muon momentum reconstruction algorithms for the CRIPT spectrometer

Pierre-Luc Drouin and David Waller

Defence R&D Canada – Ottawa

Technical Memorandum
DRDC Ottawa TM 2011-210
December 2011

Canada

Muon momentum reconstruction algorithms for the CRIPT spectrometer

Pierre-Luc Drouin
David Waller

Defence R&D Canada – Ottawa
Technical Memorandum
DRDC Ottawa TM 2011-210
December 2011

Corresponding Author

Original signed by David Waller

David Waller

Approved by

Original signed by J. Tremblay-Lutter

J. Tremblay-Lutter
Head Capabilities for Asymmetric and Radiological Defence and Simulation Section

Approved for release by

Original signed by C. McMillan

C. McMillan
DRDC Ottawa Chief Scientist

Abstract

The goal of the Cosmic Ray Inspection and Passive Tomography (CRIPT) for Special Nuclear Material (SNM) Detection project is to design, build and test a large-scale muon scattering tomography (MST) system for detecting SNM and dense radiation-shielding materials like lead. Measuring the momenta of muons on an event-by-event basis is a critical part of MST as it reduces the required detection times significantly compared to making no momentum measurements. This paper describes improved algorithms for the estimation of muon momenta. Improved algorithms were required due to modifications of the CRIPT design: the spectrometer height had to be reduced from 2.0 m to 1.0 m. After investigating several momentum estimation algorithms, a Bayesian estimator, using either flat or cosmic ray muon priors, was found to be the best. These studies also resulted in a re-design of CRIPT's muon spectrometer: the number of scattering and detector layers was reduced from four to two, and the thickness of each iron scattering layer was increased from 5 cm to 10 cm.

Résumé

L'objectif du projet Inspection et tomographie passive par rayonnements cosmiques (CRIPT, de l'anglais Cosmic Ray Inspection and Passive Tomography) pour les matières nucléaires spéciales (MNS) est de concevoir, de construire et de mettre à l'essai un système de tomographie par diffusion de muons (TDM) à grande échelle destiné à la détection des matières nucléaires spéciales (MNS) et des matériaux denses, comme le plomb, utilisés comme blindage contre le rayonnement. La mesure de la quantité de mouvement des muons événement par événement est un élément essentiel de la TDM, car elle permet de réduire de façon importante le temps de détection en comparaison d'une méthode ne faisant pas appel à une telle mesure. Le présent article décrit les algorithmes améliorés destinés à l'estimation de la quantité de mouvement des muons. De tels algorithmes améliorés étaient nécessaires en raison des modifications apportées à la conception du système CRIPT : la hauteur du spectromètre a dû être réduite de 2,0 m à 1,0 m. Après avoir évalué plusieurs algorithmes d'estimation de la quantité de mouvement, nous avons déterminé que le meilleur choix était un estimateur bayésien appliquant une loi de probabilité a priori uniforme ou correspondant aux muons engendrés par le rayonnement cosmique. Ces études ont également mené à une re-conception du spectromètre à muons du système CRIPT : nous avons fait passer de quatre à deux le nombre de couches de diffusion et de couches de détecteurs, et nous avons fait passer de 5 cm à 10 cm l'épaisseur de chaque couche de diffusion en fer.

This page intentionally left blank.

Executive summary

Muon momentum reconstruction algorithms for the CRIPT spectrometer

Pierre-Luc Drouin, David Waller; DRDC Ottawa TM 2011-210; Defence R&D Canada – Ottawa; December 2011.

Introduction: The Cosmic Ray Inspection and Passive Tomography (CRIPT) for Special Nuclear Material (SNM) Detection project is a Chemical, Biological, Radiological, Nuclear, Explosives (CBRNE) Research & Technology Initiative (CRTI) project that is investigating the effectiveness of muon scattering tomography for detecting SNM and the dense shielding that would likely surround smuggled radiological material (RAM). The goal of the CRIPT project is to design, build and test a large-scale prototype system that will be able to image air-cargo containers, and nuclear waste containers using naturally occurring cosmic-ray-induced muons. Measuring the momenta of muons on an event-by-event basis should reduce the required imaging times significantly. This paper describes improved algorithms for the estimation of muon momenta.

Previous momentum estimation algorithm: The CRIPT spectrometer measures the multiple scattering of muons through two 10 cm layers of iron. Four independent scattering angles are used to estimate the width of the scattering angle distribution and hence the momentum of the muon. The maximum likelihood (ML) algorithm that was previously developed for CRIPT worked well for a 2.0 m high spectrometer, but revised design constraints required the spectrometer height to be reduced to 1.0 m. The old algorithm produced results that had very large biases and poor resolution for muons with momentum greater than 2.0 GeV/c. This necessitated the development of an improved algorithm.

New momentum estimation algorithms: Three new types of momentum estimation algorithms were investigated: (1) Kalman filter methods, (2) an improved ML technique, and (3) a Bayesian estimator. Both extended and unscented Kalman filters were investigated but neither provided useful momentum estimators as muon scattering does not behave linearly. An improved ML technique that included an integration over the measured muon positions was superior to the old ML technique, but suffered from very long calculation times and unacceptably large biases. The Bayesian estimator performed best as it has three significant improvements over the old ML method: (a) it considers correlations between the scattering angle measurements from each layer of the spectrometer; (b) it estimates the true muon positions; and, (c) it can use a priori knowledge of the cosmic ray muon momentum spectrum to constrain the estimated muon momentum.

Results and conclusions: Simulation studies show that a Bayesian estimator provides the best results for muon momentum estimates in CRIPT's 1.0 m tall spectrometer. Using a flat muon momentum prior, all but 22.4% of the muons are successfuly fit; both the bias (-16%) and resolution ($^{+74\%}_{-16\%}$) are acceptable for performing muon scattering tomography. The fits that fail with the flat prior can be re-analyzed with a cosmic ray muon prior; none of these fits fail though the overall resolution is slightly degraded to $^{+92\%}_{-18\%}$.

Recommendations: The Bayesian estimator is the preferred algorithm for muon estimation in the CRIPT spectrometer. These simulation studies have led to the recommendation (that has already been implemented) that the new (shorter) 1.0 m high spectrometer be modified to have only two layers of 10 cm thick steel.

Sommaire

Muon momentum reconstruction algorithms for the CRIPT spectrometer

Pierre-Luc Drouin, David Waller ; DRDC Ottawa TM 2011-210 ; R & D pour la défense Canada – Ottawa ; décembre 2011.

Introduction : Le projet Inspection et tomographie passive par rayonnements cosmiques (CRIPT, de l'anglais Cosmic Ray Inspection and Passive Tomography) pour les matières nucléaires spéciales (MNS) est un projet de l'Initiative de recherche et de technologie chimique, biologique, radiologique, nucléaire et explosive (CBRNE) [IRTC] destiné à évaluer l'efficacité de la tomographie par diffusion de muons pour la détection des MNS et du blindage dense qui risque d'entourer les matières radioactives de contrebande. L'objectif du projet CRIPT est de concevoir, de construire et de mettre à l'essai un système prototype à grande échelle qui sera en mesure de fournir une imagerie des conteneurs de fret aérien et des contenants de déchets nucléaires par l'utilisation des muons générés de façon naturelle par le rayonnement cosmique. La mesure de la quantité de mouvement des muons événement par événement devrait réduire de façon importante le temps requis pour l'obtention d'images. Le présent exposé offre une description des algorithmes améliorés destinés à l'estimation de la quantité de mouvement des muons.

Ancien algorithme d'estimation de la quantité de mouvement : Le spectromètre du système CRIPT mesure la diffusion des muons à travers deux couches de fer de 10 cm d'épaisseur. Quatre angles de diffusion indépendants servent à l'estimation de la largeur de la distribution des angles de diffusion et donc à la quantité de mouvement des muons. L'algorithme de maximum de vraisemblance (MV) mis au point antérieurement pour le projet CRIPT donnait de bons résultats pour un spectromètre de 2,0 m de hauteur, mais les contraintes imposées par la nouvelle conception ont fait en sorte que la hauteur du spectromètre a dû être réduite à 1,0 m. L'ancien algorithme donnait des résultats très biaisés et présentait une faible résolution pour les muons ayant une quantité de mouvement de plus de 2,0 GeV/c, ce qui a nécessité la mise au point d'un algorithme amélioré.

Nouveaux algorithmes d'estimation de la quantité de mouvement : Nous avons évalué trois nouveaux types d'algorithme d'estimation de la quantité de mouvement : (1) des méthodes fondées sur le filtre de Kalman, (2) une technique améliorée du MV et (3) un estimateur bayésien. Nous avons évalué le filtre de Kalman étendu et le filtre de Kalman non parfumé, mais aucun des deux n'a permis d'obtenir un estimateur utile de la quantité de mouvement, car la diffusion des muons n'est pas un phénomène linéaire. Une technique améliorée du MV comprenant une intégration dans la plage des positions des muons s'est révélée supérieure à l'ancienne technique du MV, mais elle nécessitait de très longs temps

de calcul et présentait des biais d'une amplitude inacceptable. L'estimateur bayésien a été le plus efficace, car il comprenait trois améliorations importantes par rapport à l'ancienne méthode du MV : (a) il tient compte des corrélations entre les mesures de l'angle de diffusion pour chaque couche du spectromètre, (b) il permet l'estimation de la position véritable des muons et (c) il permet l'utilisation de connaissances a priori de la gamme des quantités de mouvement des muons engendrés par le rayonnement cosmique pour appliquer des contraintes aux valeurs estimées.

Résultats et conclusions : Les études de simulation montrent qu'un estimateur bayésien offre les meilleurs résultats pour l'estimation de la quantité de mouvement des muons dans le spectromètre de 1,0 m de hauteur du projet CRIPT. Avec une loi de probabilité a priori uniforme pour la quantité de mouvement des muons, seulement 22,4% de ces derniers ne sont pas ajustés correctement ; tant le biais (-16%) que la résolution ($^{+74\%}_{-16\%}$) sont acceptables pour la tomographie par diffusion de muons. Les ajustements qui ne sont pas conformes pour la loi de probabilité a priori uniforme peuvent être réanalysés pour une loi de probabilité correspondant aux muons engendrés par le rayonnement cosmique ; aucun de ces ajustements n'échoue bien que la résolution d'ensemble soit légèrement dégradée de $^{+92\%}_{-18\%}$.

Recommandations : L'estimateur bayésien est l'algorithme favori pour l'estimation de la quantité de mouvement des muons dans le spectromètre du système CRIPT. Les études de simulation ont abouti à la recommandation (déjà mise en œuvre) de modifier le nouveau spectromètre (plus court) de 1,0 m de hauteur pour qu'il ne comprenne que deux couches d'acier de 10 cm d'épaisseur.

Table of contents

List of figures

List of tables

1 Introduction

The Cosmic Ray Inspection and Passive Tomography (CRIPT) for Special Nuclear Material (SNM) Detection project is a Chemical, Biological, Radiological, Nuclear, Explosives (CBRNE) Research & Technology Initiative (CRTI) project that is investigating the effectiveness of muon scattering tomography for detecting SNM and the dense shielding that would likely surround smuggled radiological material (RAM). The goal of the CRIPT project is to design, build and test a large-scale prototype system that will be able to image air-cargo containers, and nuclear waste containers. For more details on muon scattering tomography and the CRIPT project, please see References [1, 2].

An earlier simulation study of CRIPT's muon spectrometer performance was performed in order to determine the design specifications for the spectrometer [1]. For this study, it was assumed that the spectrometer would be 2.0 m tall. Unfortunately, the height of the spectrometer will have to be no more than 1.0 m due to height constraints in the building at Carleton University [1] where CRIPT is being constructed. The reduction in height makes reliable momentum estimation more challenging, especially for higher momentum ($\gtrsim$ 2.0 GeV/c) muons as their scattering angles tend to be smaller than those of lower momentum muons.

The momentum estimation algorithm that was developed in [1] worked well when the separation between the scattering layers was 0.5 m or more, but subsequent studies (to be detailed in the following section) showed that the algorithm performance degraded severely once the layers were less than 0.25 m apart. For this reason, alternate algorithms were developed to determine if improvements could be made, and if so, what design modifications would be required for the CRIPT spectrometer to optimize performance.

After the shortcomings of the old, maximum likelihood algorithm are described in Section 2, three alternate algorithms are described in Section 3. The results of these studies are presented in Sections 2.2 and 3.5, respectively. Based on these results, the conclusions and recommendations are presented in Sections 4 and 5.

2 Previous maximum likelihood muon momentum estimation algorithm

The maximum likelihood (ML) algorithm that was developed previously for muon momentum estimation is described here briefly. For more details see Reference [1]. Figure 1

1. Although the height constraint only applies for the construction of the detector prototype, the conclusions drawn in this document regarding the relative performance of the different muon momentum reconstruction algorithms hold for other detector configurations as well.

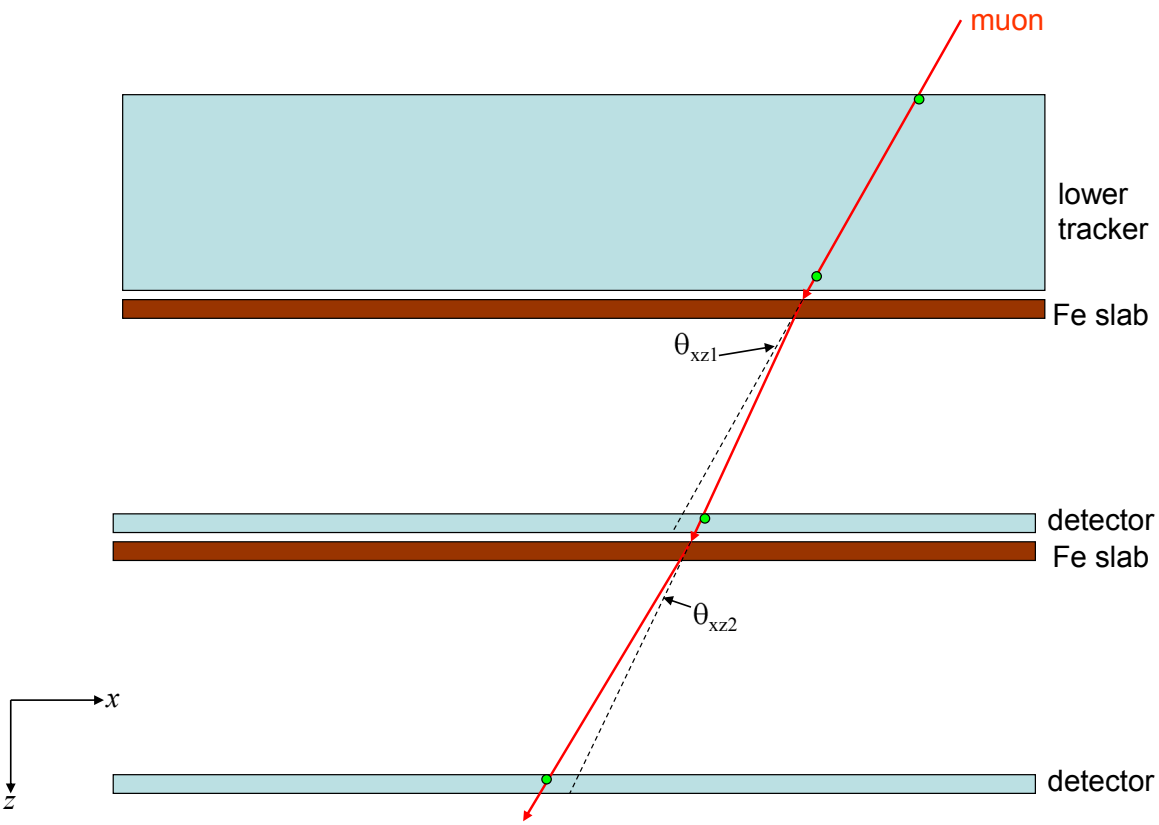

Figure 1: *A side-view of the CRIPT muon spectrometer in the x-z plane. The muon scattering angles in the x-z plane after each layer of Fe are shown by θ_{xz1} and θ_{xz2}. Two additional scattering angles can be measured in the y-z plane. The green circles in each tracker indicate muon hits. The top two trackers are not part of the spectrometer; they comprise the lower tracking module of CRIPT.*

shows a two-layer spectrometer that uses multiple Coulomb scattering through a known material in order to estimate the momentum of a muon.

2.1 Multiple Coulomb scattering of muons

The spectrometer uses layers of iron to deflect muons via multiple Coulomb scattering. The multiple scattering angles follow a distribution that is approximately Gaussian with a width, in milliradians, of

$$\theta_{\mathrm{MS}} = \frac{13.6}{\beta pc}\sqrt{\frac{L}{X_0}}\left[1+0.038\ln(L/X_0)\right], \qquad (1)$$

where β is the velocity of the muon as a fraction of the speed of light, p is the momentum of the muon in MeV/c, L is the path length of the muon through the material, and X_0 is the radiation length of the material [3]. For high-Z, high density materials, the radiation length is relatively short which leads to larger angle scattering than for less dense, low-Z materials. For L = 5 cm in Fe (X_0 = 1.76 cm), $\theta_{\mathrm{MS}} = 12$ mrad for a 2 GeV/c muon.

The multiple scattering angle and horizontal displacement of the muon within the scattering layer are strongly correlated. In the Monte Carlo simulation, the horizontal displacement, y_d, is given by

$$y_d = g_1 L\theta_{\mathrm{MS}}/\sqrt{12} + g_2 L\theta_{\mathrm{MS}}/2, \tag{2}$$

where g_1 and g_2 are independent, unit Gaussian random numbers, θ_{MS} is the width of the scattering angle distribution (from Equation 1), and L is the path length of the muon through the material. The correlation is achieved by setting the multiple scattering angle equal to $g_2\theta_{\mathrm{MS}}$.

2.2 Previous maximum likelihood algorithm

For a muon that passes through the spectrometer, two independent, orthogonal scattering angles are measured after each scattering layer. For simplicity we define these angles in the spectrometer's x-z and y-z planes (z points down to the ground). Using the known value of X_0 for Fe and the estimated path length of the muon in the absorber, L, Equation 1 can be re-arranged to estimate $1/p$.

An estimate of $1/p$ was provided by a maximum likelihood fit to the scattering angle data. The measured multiple scattering angles in the x-z and y-z planes, $\theta_{xz[yz]}$, are then compared to a Gaussian distribution

$$P(\theta_{xz[yz]}) = \frac{1}{\sqrt{2\pi}\theta} e^{\frac{-\theta^2_{xz[yz]}}{2\theta^2}} \tag{3}$$

whose width, $\theta = \sqrt{\theta^2_{\mathrm{MS}} + \sigma^2_{\theta_{xz[yz]}}}$, depends on θ_{MS} and the uncertainty in the scattering angle measurement, $\sigma_{\theta_{xz[yz]}}$ in the x-z[y-z] plane. The value of $1/p$ (and corresponding β) that minimizes the negative log likelihood function

$$-\log(\mathcal{L}) = -\left[\sum_{i=1}^{N} \log(P(\theta_{xz})) + \sum_{i=1}^{N} \log(P(\theta_{yz}))\right] \tag{4}$$

for the N scattering layers is taken as the estimate of $1/p$: $1/p_{\mathrm{fit}}$.

Results from the previous study with a 2.0 m high spectrometer showed that there was a 12% bias to the fitted inverse momentum, $1/p_{\mathrm{fit}}$. This bias was largely independent of muon momentum (0.5 GeV/$c \leq p_{\mathrm{fit}} \leq$ 10.0 GeV/c) so a correction could be applied to $1/p_{\mathrm{fit}}$ to yield good agreement with the true inverse momentum, $1/p_{\mathrm{true}}$. The $\sim 2\%$

Table 1: *The results of $1/p_{fit}$ with the old algorithm for a two-layer, 1.0 m tall spectrometer with 2 mm hit resolution and 5 cm thick Fe scattering layers. The difference between $1/p_{true}$ and $1/p_{fit}$ is not constant across this range of momenta so a correction can not be applied without introducing significant extra uncertainty.*

p_{true} GeV/c	$1/p_{true}$ c/GeV	$< 1/p_{fit} >$ c/GeV	RMS($1/p_{fit}$) c/GeV	Bias %	Resolution %
0.5	2.0	1.75	0.65	-13	37
1.0	1.0	0.91	0.38	-9	41
2.0	0.5	0.52	0.27	4	52
5.0	0.2	0.32	0.24	60	75
10.0	0.1	0.28	0.24	180	85

Table 2: *The results of $1/p_{fit}$ with the old algorithm for a four-layer, 1.0 m tall spectrometer with 2 mm hit resolution and 5 cm thick Fe scattering layers. Above 1.0 GeV/c, it is virtually impossible to estimate the muon momentum reliably.*

p_{true} GeV/c	$1/p_{true}$ c/GeV	$< 1/p_{fit} >$ c/GeV	RMS($1/p_{fit}$) c/GeV	Bias %	Resolution %
0.5	2.0	2.54	0.84	27	33
1.0	1.0	1.87	0.87	87	47
2.0	0.5	1.64	0.91	228	56
5.0	0.2	1.56	0.94	680	60
10.0	0.1	1.55	0.94	1450	61

bias that remained after this correction was negligible compared to the $\sim$ 37% resolution of the measurements. The 12% bias was shown to be due to the use of the estimated scattering angles, instead of the *true* scattering angles; the bias was reduced to -2% if the true scattering angles were used instead.

Unfortunately, reducing the height of the spectrometer to 1.0 m caused the size of the bias to increase in a non-linear fashion, especially if a four-layer spectrometer was assumed. The reason for the poor performance of the old algorithm is due to two factors:

1. the assumption that the Gaussian distribution on the position measurement uncertainties translates into Gaussian uncertainties for the scattering angles,
2. the fact that the model only considers the position measurement from the previous (above) layer to calculate the initial muon direction for a given scattering layer rather than correlating muon direction between the layers.

Table 1 shows how the the bias becomes worse for a two-layer spectrometer as the muon momentum increases. Table 2 shows that the performance is even worse when four layers are employed.

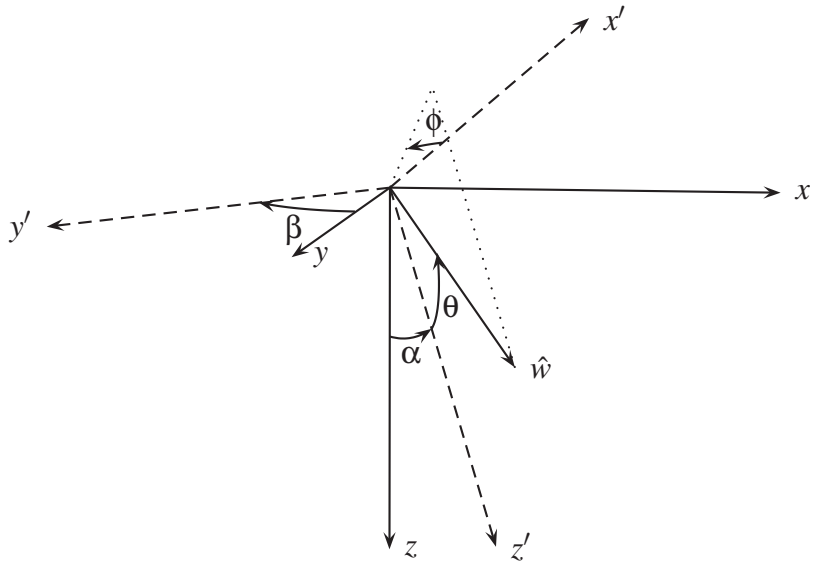

Figure 2: *Angles and systems of coordinates used to describe muon trajectory through the detector.*

In light of the very poor performance of the old algorithm with a 1.0 m high spectrometer, it was clear that an improved muon momentum estimation algorithm was required.

3 New muon momentum estimation algorithms

3.1 Setting up the algebra for the new estimator

If one defines a Cartesian coordinate system (x,y,z) fixed with respect to the detector, where the x-y plane is parallel with the detector plane and whose axes are aligned with the axes of the detector strips. In this coordinate system, the z axis points downward. Figure 2 shows the complete set of coordinate systems and angles that are used in this section. Now a Cartesian coordinate system (x',y',z') is defined, whose y' axis is in x-y plane and whose z' axis makes an angle α with respect to the z axis. The orientation of the coordinate system is chosen such that $0 \leq \alpha \leq \frac{\pi}{2}$ and that the projection along z for both the x' and z' axes is negative. If the y' axis makes an angle β in the counter-clockwise direction with respect to the y axis for the z axis pointing toward the observer, a set of coordinates (x,y,z), as a function of coordinates (x',y',z'), is given by

$$\begin{bmatrix} x \\ y \\ z \end{bmatrix} = \begin{bmatrix} \cos\alpha\cos\beta & -\sin\beta & \sin\alpha\cos\beta \\ \cos\alpha\sin\beta & \cos\beta & \sin\alpha\sin\beta \\ -\sin\alpha & 0 & \cos\alpha \end{bmatrix} \begin{bmatrix} x' \\ y' \\ z' \end{bmatrix}. \tag{5}$$

Angles α and β are defined, such that the z' axis points in the incident direction of the muon

on the steel plate. If the scattered muon makes an angle θ with respect to the z' axis and if the projection of this scatter direction in the x'-y' plane makes an angle ϕ in the counter-clockwise direction with respect to the x' axis for the z' axis pointing toward the observer, the scatter direction $\hat{w}$, in the (x', y', z') coordinate system, is thus expressed as

$$\hat{w} = \begin{bmatrix} \cos\phi\sin\theta \\ \sin\phi\sin\theta \\ \cos\theta \end{bmatrix}_{(x',y',z')} \tag{6}$$

From (5) and (6), the scatter direction $\hat{w}$ in the (x, y, z) coordinate system is thus expressed as

$$\hat{w} = \begin{bmatrix} \cos\alpha\cos\beta\cos\phi\sin\theta - \sin\beta\sin\phi\sin\theta + \sin\alpha\cos\beta\cos\theta \\ \cos\alpha\sin\beta\cos\phi\sin\theta + \cos\beta\sin\phi\sin\theta + \sin\alpha\sin\beta\cos\theta \\ -\sin\alpha\cos\phi\sin\theta + \cos\alpha\cos\theta \end{bmatrix}_{(x,y,z)} \tag{7}$$

Now a detector layer is parameterised using a steel plate thickness t, a measurement in x at a distance d_a above the plate (from the top surface), another x measurement at a distance d_b below the plate (from the bottom surface) and y measurements at a distance Δ_m below the x measurements. Figure 3 shows this parameterisation. The direction vectors for a muon through the layer are given (using (5) and (6)) by

$$\hat{v} = \begin{bmatrix} 0 \\ 0 \\ 1 \end{bmatrix}_{(x',y',z')} = \begin{bmatrix} \sin\alpha\cos\beta \\ \sin\alpha\sin\beta \\ \cos\alpha \end{bmatrix}_{(x,y,z)} \tag{8}$$

$$\hat{s} = \begin{bmatrix} \cos\alpha\cos\beta\cos\eta\sin\psi - \sin\beta\sin\eta\sin\psi + \sin\alpha\cos\beta\cos\psi \\ \cos\alpha\sin\beta\cos\eta\sin\psi + \cos\beta\sin\eta\sin\psi + \sin\alpha\sin\beta\cos\psi \\ -\sin\alpha\cos\eta\sin\psi + \cos\alpha\cos\psi \end{bmatrix}_{(x,y,z)} \tag{9}$$

$$\hat{w} = \begin{bmatrix} \cos\alpha\cos\beta\cos\phi\sin\theta - \sin\beta\sin\phi\sin\theta + \sin\alpha\cos\beta\cos\theta \\ \cos\alpha\sin\beta\cos\phi\sin\theta + \cos\beta\sin\phi\sin\theta + \sin\alpha\sin\beta\cos\theta \\ -\sin\alpha\cos\phi\sin\theta + \cos\alpha\cos\theta \end{bmatrix}_{(x,y,z)}, \tag{10}$$

where $\hat{v}$ is the direction vector of the incident muon, $\hat{s}$ is the direction vector of its deflected displacement in the steel plate and where $\hat{w}$ is its direction after exiting the steel plate. Angles ψ and η give the direction of $\hat{s}$ with respect to the (x', y', z') coordinate system, similarly to angles θ and ϕ for the direction of $\hat{w}$. Since the z components of the corresponding displacement vectors $\vec{v}$, $\vec{s}$ and $\vec{w}$ are known to be

$$\begin{aligned} v_{xz} &= d_a, & s_{xz} &= t, & w_{xz} &= d_b \\ v_{yz} &= (d_a - \Delta_m), & s_{yz} &= t, & w_{yz} &= (d_b + \Delta_m), \end{aligned}$$

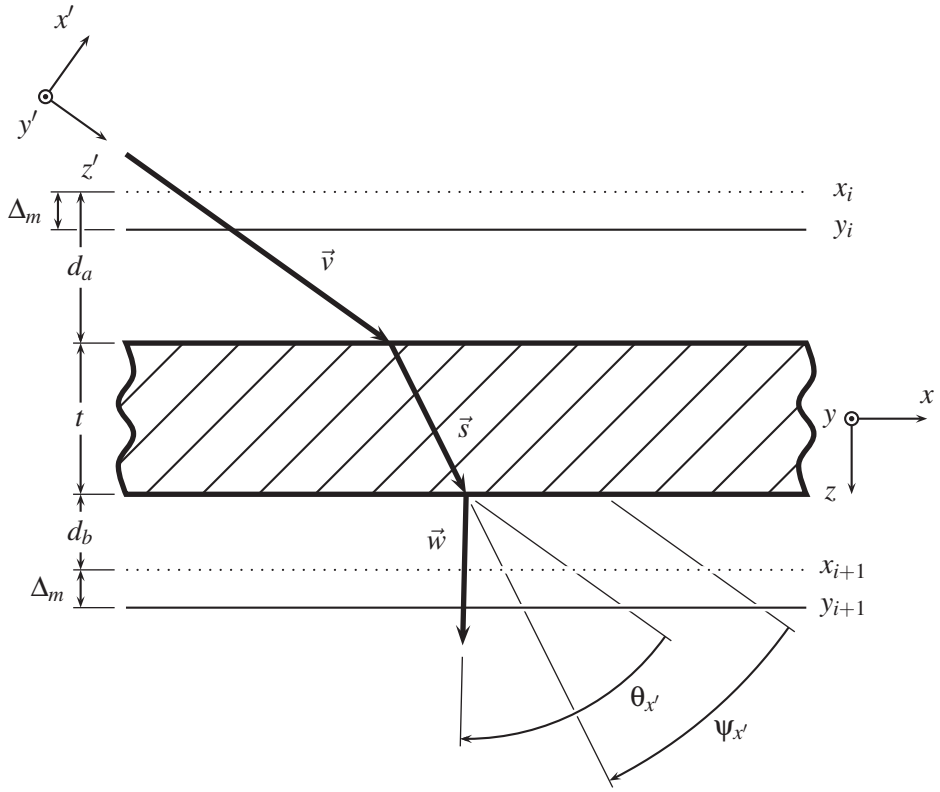

Figure 3: *Parameterisation of the detector geometry.*

for the x and y measurements respectively, the true x and y components of the muon displacement between two detector layers are thus given by

$$\begin{aligned}
\Delta x &= \frac{\hat{v}_x}{\hat{v}_z}v_{xz} + \frac{\hat{s}_x}{\hat{s}_z}s_{xz} + \frac{\hat{w}_x}{\hat{w}_z}w_{xz} \\
&= d_a \tan\alpha\cos\beta + t\frac{\cos\alpha\cos\beta\cos\eta\sin\psi - \sin\beta\sin\eta\sin\psi + \sin\alpha\cos\beta\cos\psi}{\cos\alpha\cos\psi - \sin\alpha\cos\eta\sin\psi} \\
&\quad + d_b\frac{\cos\alpha\cos\beta\cos\phi\sin\theta - \sin\beta\sin\phi\sin\theta + \sin\alpha\cos\beta\cos\theta}{\cos\alpha\cos\theta - \sin\alpha\cos\phi\sin\theta} \qquad (11) \\
\Delta y &= \frac{\hat{v}_y}{\hat{v}_z}v_{yz} + \frac{\hat{s}_y}{\hat{s}_z}s_{yz} + \frac{\hat{w}_y}{\hat{w}_z}w_{yz} \\
&= (d_a - \Delta_m)\tan\alpha\sin\beta + t\frac{\cos\alpha\sin\beta\cos\eta\sin\psi + \cos\beta\sin\eta\sin\psi + \sin\alpha\sin\beta\cos\psi}{\cos\alpha\cos\psi - \sin\alpha\cos\eta\sin\psi} \\
&\quad + (d_b + \Delta_m)\frac{\cos\alpha\sin\beta\cos\phi\sin\theta + \cos\beta\sin\phi\sin\theta + \sin\alpha\sin\beta\cos\theta}{\cos\alpha\cos\theta - \sin\alpha\cos\phi\sin\theta}. \qquad (12)
\end{aligned}$$

(11) and (12) thus give the expectation values (that is to say, without effects due to position measurement uncertainties) for the difference between the position measurements for two consecutive layers, given the direction parameters $(\alpha, \beta, \theta, \phi, \psi, \eta)$, and the detector geometry parameters (d_a, d_b, Δ_m, t).

If it is now assumed that both the scattering angle θ and the deviation angle ψ are small

and that $\theta_{x'} \approx \cos\phi\sin\theta$, $\theta_{y'} \approx \sin\phi\sin\theta$, $\psi_{x'} \approx \cos\eta\sin\psi$ and $\psi_{y'} \approx \sin\eta\sin\psi$ are defined as the projections onto the x' and y' axes of the θ and ψ angles respectively, (11) and (12) can be rewritten as

$$\begin{aligned}\Delta x &\approx d_a\tan\alpha\cos\beta + t\frac{\cos\alpha\cos\beta\psi_{x'} - \sin\beta\psi_{y'} + \sin\alpha\cos\beta}{\cos\alpha - \sin\alpha\psi_{x'}} \\ &\quad + d_b\frac{\cos\alpha\cos\beta\theta_{x'} - \sin\beta\theta_{y'} + \sin\alpha\cos\beta}{\cos\alpha - \sin\alpha\theta_{x'}} \qquad (13)\\ \Delta y &\approx (d_a - \Delta_m)\tan\alpha\sin\beta + t\frac{\cos\alpha\sin\beta\psi_{x'} + \cos\beta\psi_{y'} + \sin\alpha\sin\beta}{\cos\alpha - \sin\alpha\psi_{x'}} \\ &\quad + (d_b + \Delta_m)\frac{\cos\alpha\sin\beta\theta_{x'} + \cos\beta\theta_{y'} + \sin\alpha\sin\beta}{\cos\alpha - \sin\alpha\theta_{x'}}. \qquad (14)\end{aligned}$$

Under a Gaussian approximation for the scattering and deviation angles, the following expressions to generate both angles can be obtained from [3]:

$$\begin{aligned}\theta_{x'} &= z_{1x'}\theta_0 \qquad (15)\\ \psi_{x'} &= \gamma\theta_{x'} + \xi z_{2x'}\theta_0 \qquad (16)\\ \theta_{y'} &= z_{1y'}\theta_0 \qquad (17)\\ \psi_{y'} &= \gamma\theta_{y'} + \xi z_{2y'}\theta_0 \qquad (18)\\ \gamma &\equiv \frac{1}{2} \qquad (19)\\ \xi &\equiv \frac{1}{\sqrt{12}} \qquad (20)\\ \theta_0 &\equiv \frac{13.6\text{ MeV}}{p^2}\sqrt{\frac{|\vec{s}|}{X_{0\text{Fe}}}(p^2 + m_\mu^2)}\left[1 + 0.038\log\left(\frac{|\vec{s}|}{X_{0\text{Fe}}}\right)\right], \qquad (21)\end{aligned}$$

where $z_{1x'}$, $z_{2x'}$, $z_{1y'}$ and $z_{2y'}$ are independent $N(0,1)$ Gaussian random variables, where p is the muon momentum in MeV, where m_μ is the muon mass in MeV, where $X_{0\text{Fe}}$ is the radiation length of steel in cm and where $|\vec{s}|$ is the effective displacement length of the muon in the steel plate in cm. Neglecting the effect of the deviation in the plate on the effective displacement length, $|\vec{s}|$ can be approximated by

$$|\vec{s}| = \frac{t}{\cos\alpha - \sin\alpha\psi_{x'}} \approx \frac{t}{\cos\alpha}. \qquad (22)$$

From (13) to (20), it can be seen that random variables $z_{2x'}$ and $z_{2y'}$ normally have small effects on Δx and Δy, compared to $z_{1x'}$ and $z_{1y'}$, because the former variables only affect the propagation of the muons through the steel plate, while the latter also affect the propagation between the steel plate and the detector plane below and that $\xi = \frac{\gamma}{\sqrt{3}}$. So except for a very particular detector geometry where $d_b < 2t$, the above equations can be simplified using

the approximation

$$\psi_{x'} \approx \gamma\theta_{x'} \tag{23}$$
$$\psi_{y'} \approx \gamma\theta_{y'} \tag{24}$$

without creating significant fit biases. Using the same small scattering and deviation angle approximation as previously, (13) and (14) can thus now be rewritten as

$$\begin{aligned}\Delta x \approx\ & d_a \tan\alpha\cos\beta + \{\cos\alpha[\cos\alpha - \sin\alpha\theta_{x'}(\gamma+1)]\}^{-1} \times \\ & \{t\left[\gamma\cos\alpha(\cos\alpha\cos\beta\theta_{x'} - \sin\beta\theta_{y'}) + \sin\alpha\cos\beta(\cos\alpha - \sin\alpha\theta_{x'})\right] + \\ & d_b\left[\cos\alpha(\cos\alpha\cos\beta\theta_{x'} - \sin\beta\theta_{y'}) + \sin\alpha\cos\beta(\cos\alpha - \gamma\sin\alpha\theta_{x'})\right]\}\end{aligned} \tag{25}$$

$$\begin{aligned}\Delta y \approx\ & (d_a - \Delta_m)\tan\alpha\sin\beta + \{\cos\alpha[\cos\alpha - \sin\alpha\theta_{x'}(\gamma+1)]\}^{-1} \times \\ & \{t\left[\gamma\cos\alpha(\cos\alpha\sin\beta\theta_{x'} + \cos\beta\theta_{y'}) + \sin\alpha\sin\beta(\cos\alpha - \sin\alpha\theta_{x'})\right] + \\ & (d_b + \Delta_m)\left[\cos\alpha(\cos\alpha\sin\beta\theta_{x'} + \cos\beta\theta_{y'}) + \sin\alpha\sin\beta(\cos\alpha - \gamma\sin\alpha\theta_{x'})\right]\}.\end{aligned} \tag{26}$$

Equations (25) and (26) are linear in $\theta_{x'}$ and $\theta_{y'}$, so analytical expressions for the scattering angles can be extracted easily (although they are not very elegant).

Regarding the relation between the direction vectors for consecutive layers, expressions can be obtained using (8), (10) and the relation $\vec{v}' = \vec{w}$. This thus gives

$$\begin{bmatrix} \sin\alpha'\cos\beta' \\ \sin\alpha'\sin\beta' \\ \cos\alpha' \end{bmatrix} \approx \begin{bmatrix} \cos\alpha\cos\beta\theta_{x'} - \sin\beta\theta_{y'} + \sin\alpha\cos\beta \\ \cos\alpha\sin\beta\theta_{x'} + \cos\beta\theta_{y'} + \sin\alpha\sin\beta \\ -\sin\alpha\theta_{x'} + \cos\alpha \end{bmatrix}. \tag{27}$$

Given that $0 \leq \alpha \leq \frac{\pi}{2}$, the expressions for the new values of the angles (or their trigonometric functions) are thus

$$\cos\alpha' = -\sin\alpha\theta_{x'} + \cos\alpha \tag{28}$$
$$\sin\alpha' = \sqrt{1 - \cos^2\alpha'} \tag{29}$$
$$\begin{aligned}\beta' = \ & \arctan(\cos\alpha\sin\beta\theta_{x'} + \cos\beta\theta_{y'} + \sin\alpha\sin\beta, \\ & \cos\alpha\cos\beta\theta_{x'} - \sin\beta\theta_{y'} + \sin\alpha\cos\beta),\end{aligned} \tag{30}$$

where $\arctan(y,x)$ is the inverse trigonometric function that returns an angle in the range $[-\pi,\pi]$ depending on the sign of its arguments.

3.2 Bayesian estimator

The first method that is used to reconstruct the muon momentum uses a Bayesian estimator. This method should allow one to extract the muon momentum while using all information available, including correlations between the different detector layers. The Bayesian probability density function (PDF) is written as

$$\begin{aligned} f(\text{model}|\text{sample}) &= f(p_0,\vec{p},x_{0_t},\phi_{0_t},\vec{x}_t|x_{0_m},\phi_{0_m},\vec{x}_m) \\ &= f(p_0,\vec{p}|x_{0_t},\phi_{0_t},\vec{x}_t,x_{0_m},\phi_{0_m},\vec{x}_m) f(x_{0_t},\phi_{0_t},\vec{x}_t|x_{0_m},\phi_{0_m},\vec{x}_m) \\ &= f(p_0,\vec{p}|x_{0_t},\phi_{0_t},\vec{x}_t) f(x_{0_t},\phi_{0_t},\vec{x}_t|x_{0_m},\phi_{0_m},\vec{x}_m), \end{aligned} \tag{31}$$

where
n : Number of detector planes
x_{it} : True position on detector plane i ($1 \leq i \leq n$). $\vec{x}_t \equiv (x_{1t}, \ldots, x_{nt})$
x_{im}: Measured position on detector plane i. $\vec{x}_m \equiv (x_{1m}, \ldots, x_{nm})$
ϕ_{it} : True angle with z axis after the muon exits the steel plate of detector plane i.
p_i : Momentum for detector plane i. $\vec{p} \equiv (p_1, \ldots, p_n)$
x_0 : Initial position.
ϕ_0 : Initial angle with z axis.
p_0 : Initial momentum.

In the above expression, positions and angles should be each interpreted as 2D entities. $f(p_0, \vec{p}|x_{0t}, \phi_{0t}, \vec{x}_t)$ is the PDF that gives the probability of the set of angular momenta $(p_0, \vec{p})$, given the true positions and directions $(x_{0t}, \phi_{0t}, \vec{x}_t)$. It was simplified from the PDF $f(p_0, \vec{p}|x_{0t}, \phi_{0t}, \vec{x}_t, x_{0m}, \phi_{0m}, \vec{x}_m)$ using the fact that measured positions and directions do not provide any additional information in determining momenta if the true positions and directions are known. From Bayes' theorem, $f(p_0, \vec{p}|x_{0t}, \phi_{0t}, \vec{x}_t)$ is then rewritten as

$$f(p_0, \vec{p}|x_{0t}, \phi_{0t}, \vec{x}_t) = f(\vec{x}_t|p_0, \vec{p}, x_{0t}, \phi_{0t}) \frac{f(p_0, \vec{p}|x_{0t}, \phi_{0t})}{f(\vec{x}_t|x_{0t}, \phi_{0t})}, \tag{32}$$

Now using Bayes' theorem with $f(x_{0t}, \phi_{0t}, \vec{x}_t|x_{0m}, \phi_{0m}, \vec{x}_m)$,

$$\begin{aligned} f(x_{0t}, \phi_{0t}, \vec{x}_t|x_{0m}, \phi_{0m}, \vec{x}_m) &= f(x_{0m}, \phi_{0m}, \vec{x}_m|x_{0t}, \phi_{0t}, \vec{x}_t) \frac{f(x_{0t}, \phi_{0t}, \vec{x}_t)}{f(x_{0m}, \phi_{0m}, \vec{x}_m)} \\ &= f(x_{0m}, \phi_{0m}|x_{0t}, \phi_{0t}) f(\vec{x}_m|\vec{x}_t) \times \\ &\quad \frac{f(x_{0t}, \phi_{0t}) f(\vec{x}_t|x_{0t}, \phi_{0t})}{f(x_{0m}, \phi_{0m}, \vec{x}_m)}. \end{aligned} \tag{33}$$

(31) to (33) can now be combined to give

$$\begin{aligned} f(\text{model}|\text{sample}) &= f(x_{0m}, \phi_{0m}|x_{0t}, \phi_{0t}) \left[\prod_{i=1}^{n} f(x_{im}|x_{it}) \right] \frac{f(x_{0t}, \phi_{0t}) f(p_0, \vec{p}|x_{0t}, \phi_{0t})}{f(x_{0m}, \phi_{0m}, \vec{x}_m)} \times \\ &\quad f(\vec{x}_t|p_0, \vec{p}, x_{0t}, \phi_{0t}). \end{aligned} \tag{34}$$

$f(\vec{x}_t|p_0, \vec{p}, x_{0t}, \phi_{0t})$ is rewritten as

$$f(\vec{x}_t|p_0, \vec{p}, x_{0t}, \phi_{0t}) = \prod_{i=1}^{n} f(x_{it}|p_0, \vec{p}, x_{0t}, \phi_{0t}, x_{1t}, \ldots, x_{i-1t}). \tag{35}$$

$f(x_{it}|p_0,\vec{p},x_{0_t},\phi_{0_t},x_{1_t},\ldots,x_{i-1_t})$ is equivalent to

$$\begin{aligned}
f(x_{it}|p_0,\vec{p},x_{0_t},\phi_{0_t},x_{1_t},\ldots,x_{i-1_t}) &= \int f(x_{it},\phi_{i-1_t}|p_0,\vec{p},x_{0_t},\phi_{0_t},x_{1_t},\ldots,x_{i-1_t})d\phi_{i-1_t} \\
&= \int \Big\{ f(x_{it}|p_0,\vec{p},x_{0_t},\phi_{0_t},x_{1_t},\ldots,x_{i-1_t},\phi_{i-1_t}) \times \\
&\quad f(\phi_{i-1_t}|p_0,\vec{p},x_{0_t},\phi_{0_t},x_{1_t},\ldots,x_{i-1_t}) \Big\} d\phi_{i-1_t} \\
&= \int \Big\{ f(x_{it}|p_{i-1},p_i,x_{i-1_t},\phi_{i-1_t}) \times \\
&\quad f(\phi_{i-1_t}|p_0,\vec{p},x_{0_t},\phi_{0_t},x_{1_t},\ldots,x_{i-1_t}) \Big\} d\phi_{i-1_t} \\
&= \int \Bigg\{ f(x_{it}-x_{i-1_t}|p_{i-1},p_i,\phi_{i-1_t}) \times \\
&\quad \prod_{j=1}^{i-1} f(\phi_{j_t}|p_{j-1},p_j,x_{j_t}-x_{j-1_t},\phi_{j-1_t}) \Bigg\} d\phi_{1_t}\ldots d\phi_{j-1_t} \quad (36)
\end{aligned}$$

due to the properties of the x_{i_t} PDF which can only depend on p_{i-1}, p_i, x_{i-1_t} and ϕ_{i-1_t}, and to the ones of the ϕ_{i_t} PDF, which can only depend on the same variables, plus x_{i_t}. The final expression was obtained by "unmarginalising" the initial PDF recursively. From (34) to (36), an exact expression for the Bayesian PDF is thus given by

$$\begin{aligned}
f(\text{model}|\text{sample}) &= f(x_{0_m},\phi_{0_m}|x_{0_t},\phi_{0_t}) \frac{f(x_{0_t},\phi_{0_t}) f(p_0,\vec{p}|x_{0_t},\phi_{0_t})}{f(x_{0_m},\phi_{0_m},\vec{x}_m)} \times \\
&\quad \prod_{i=1}^{n} f(x_{i_m}-x_{i_t}) \int \Bigg\{ f(x_{it}-x_{i-1_t}|p_{i-1},p_i,\phi_{i-1_t}) \times \\
&\quad \prod_{j=1}^{i-1} f(\phi_{j_t}|p_{j-1},p_j,x_{j_t}-x_{j-1_t},\phi_{j-1_t}) \Bigg\} d\phi_{1_t}\ldots d\phi_{j-1_t}. \quad (37)
\end{aligned}$$

Two changes are then made to the above function without introducing any approximation. The first one is to drop the factor $f(x_{0_m},\phi_{0_m},\vec{x}_m)$ from the denominator, since its expression does not depend on any of the fit parameters and dropping it does not affect the position of the maximum. The second change consists in performing the variable transformation $\phi_{0_t} \rightarrow \phi_{0_t}(x_{-1_t},x_{0_t})$, where x_{-1_t} represents the other pair of measured coordinates from CRIPT's lower tracker that is used to estimate the initial direction. This change allows one to express the PDF $f(x_{0_m},\phi_{0_m}|x_{0_t},\phi_{0_t})$ more easily, since as the initial direction is estimated using a pair of measured positions, including the one used to estimate the initial position, the variables of this PDF are thus correlated and the marginal PDFs along the direction axes are non-Gaussian. $f(x_{0_m},\phi_{0_m}|x_{0_t},\phi_{0_t})$ is thus rewritten as

$$\begin{aligned}
f(x_{0_m},\phi_{0_m}|x_{0_t},\phi_{0_t}) &\rightarrow f(x_{0_m},\phi_{0_m}((x_{-1_m},x_{0_m})|x_{0_t},\phi_{0_t}((x_{-1_t},x_{0_t})) \\
&\rightarrow f(x_{-1_m}-x_{-1_t},x_{0_m}-x_{0_t}) \\
&\rightarrow f(x_{-1_m}-x_{-1_t}) f(x_{0_m}-x_{0_t}), \quad (38)
\end{aligned}$$

where $f(x_{-1_m} - x_{-1_t})$ and $f(x_{0_m} - x_{0_t})$ are the same position measurement uncertainty PDFs as $f(x_{i_m} - x_{i_t})$, except that they are respectively evaluated for the extra layer used to measure the initial muon direction and the layer used to measure both the initial muon direction and position. Note that converting from the original PDF to the new one involves the computation of a Jacobian, but the usage of this Jacobian is irrelevant in the context of the maximisation of the Bayesian PDF, since the Jacobian only depends on measured quantities and not on the fit parameters. The PDF thus simplifies to

$$\begin{aligned} f(\text{model}|\text{sample}) \propto\ & f(x_{-1_m} - x_{-1_t}) f(x_{0_m} - x_{0_t}) f(x_{0_t}, \phi_{0_t}) f(p_0, \vec{p}|x_{0_t}, \phi_{0_t}) \times \\ & \prod_{i=1}^{n} f(x_{i_m} - x_{i_t}) \int \left\{ f(x_{i_t} - x_{i-1_t}|p_{i-1}, p_i, \phi_{i-1_t}) \times \right. \\ & \left. \prod_{j=1}^{i-1} f(\phi_{j_t}|p_{j-1}, p_j, x_{j_t} - x_{j-1_t}, \phi_{j-1_t}) \right\} d\phi_{1_t} \ldots d\phi_{j-1_t}. \end{aligned} \tag{39}$$

The expression (39) is exact since it was obtained without using any approximation. However, it can be impractical to use, due to the non-analytical integrals to be performed. If the last approximation that was introduced in the previous section, that is, a 100% correlation between the deviation and scattering angles, is now used with the Bayesian PDF, an important simplification occurs. Effectively, using such an approximation makes the direction ϕ_{j_t} to be defined exactly when ϕ_{j-1_t}, p_{j-1}, p_j, x_{j-1_t} and x_{j_t} are known. The PDFs $f(\phi_{j_t}|p_{j-1}, p_j, x_{j-1_t}, \phi_{j-1_t}, x_{j_t})$ thus simply become

$$\begin{aligned} f(\phi_{j_t}|p_{j-1}, p_j, x_{j-1_t}, \phi_{j-1_t}, x_{j_t}) &= \delta(\phi_{j_t} - \phi_{j_t}(\phi_{j-1_t}, p_{j-1}, p_j, x_{j-1_t}, x_{j_t})) \\ &= \delta(\phi_{j_t} - \phi_{j_t}(\phi_{0_t}, x_{0_t}, \ldots, x_{j_t}, p_0, \ldots, p_j)), \end{aligned} \tag{40}$$

where $\delta()$ is the Dirac delta function and where $\phi_{j_t}(\phi_{0_t}, x_{0_t}, \ldots, x_{j_t}, p_0, \ldots, p_j)$ is the function that provides the unique value of ϕ_{j_t} corresponding to its arguments. Also, a simplification can be introduced regarding the momentum p, which can be approximated to decrease in a deterministic way, given the incident angle of the muon. Under these two approximations,

$$\begin{aligned} f(\text{model'}|\text{sample}) \propto\ & f(x_{-1_m} - x_{-1_t}) f(x_{0_m} - x_{0_t}) f(x_{0_t}, \phi_{0_t}) f(p_0|x_{0_t}, \phi_{0_t}) \times \\ & \prod_{i=1}^{n} f(x_{i_m} - x_{i_t}) f(x_{i_t} - x_{i-1_t}|p_{i-1}, \phi_{i-1_t}), \end{aligned} \tag{41}$$

with $p_{i-1} \approx p_{i-1}(\phi_{0_t}, x_{0_t}, \ldots, x_{i-1_t}, p_0)$ and $\phi_{i_t} \approx \phi_{i_t}(\phi_{0_t}, x_{0_t}, \ldots, x_{i_t}, p_0)$. The above expression was obtained using

$$\begin{aligned} f(p_0, \vec{p}|x_{0_t}, \phi_{0_t}) &= f(p_0|x_{0_t}, \phi_{0_t}) f(\vec{p}|x_{0_t}, \phi_{0_t}) \\ &= f(p_0|x_{0_t}, \phi_{0_t}) \prod_{i=1}^{n} \delta[p_i - p_i(\phi_{0_t}, x_{0_t}, \ldots, x_{i-1_t}, p_0)] \end{aligned} \tag{42}$$

and then by defining a new model $f(\text{model'}|\text{sample})$ that does not have free parameters for the p_i momenta. This is achieved by integrating the PDF $f(\text{model}|\text{sample})$ over these momenta.

An expression for the PDF $f(x_{it} - x_{i-1t}|p_{i-1}, \phi_{i-1t})$ can now be found by using the equations that have been developed in the previous section and a transformation of variable. Using the notation from the Section 3.1, this PDF is given by

$$f(x_{it} - x_{i-1t}|p_{i-1}, \phi_{i-1t}) = f(\Delta x_i, \Delta y_i|p_{i-1}, \alpha_{i-1}, \beta_{i-1}), \tag{43}$$

where indices have been added to the variable names to identify the detector layer to which they are associated. From probability theory[4], the PDF $f(\Delta x_i, \Delta y_i|p_{i-1}, \alpha_{i-1}, \beta_{i-1})$ can be obtained using

$$f(\Delta x_i, \Delta y_i|p_{i-1}, \alpha_{i-1}, \beta_{i-1}) = \frac{f(\theta_{x'i}(\Delta x_i, \Delta y_i, \alpha_{i-1}, \beta_{i-1}), \theta_{y'i}(\Delta x_i, \Delta y_i, \alpha_{i-1}, \beta_{i-1})|p_{i-1}, \alpha_{i-1})}{J_i}, \tag{44}$$

where J_i is the Jacobian

$$J_i = \begin{vmatrix} \frac{\partial \Delta x_i}{\partial \theta_{x'i}} & \frac{\partial \Delta x_i}{\partial \theta_{y'i}} \\ \frac{\partial \Delta y_i}{\partial \theta_{x'i}} & \frac{\partial \Delta y_i}{\partial \theta_{y'i}} \end{vmatrix} \tag{45}$$

and where $\theta_{x'i}(\Delta x_i, \Delta y_i, \alpha_{i-1}, \beta_{i-1})$ and $\theta_{y'i}(\Delta x_i, \Delta y_i, \alpha_{i-1}, \beta_{i-1})$ are the scattering angles for detector plane i, as computed after analytically solving the linear equations (25) and (26) for $\theta_{x'}$ and $\theta_{y'}$. $f(\theta_{x'}, \theta_{y'}|p, \alpha)$ is the PDF for two independent variables, so it can be written as

$$f(\theta_{x'}, \theta_{y'}|p, \alpha) = f(\theta_{x'}|\theta_0(p, \alpha)) f(\theta_{y'}|\theta_0(p, \alpha)), \tag{46}$$

where both marginal PDFs $f(\theta_{x'}|\theta_0)$ and $f(\theta_{y'}|\theta_0)$ are $N(0, \theta_0^2)$, under the Gaussian approximation mentioned earlier. θ_0 has been expressed by (21) and (22). From (25) and (26), the Jacobian elements are given by

$$\frac{\partial \Delta x}{\partial \theta_{x'}} = \frac{(\gamma t + d_b)[\cos\beta - \sin\alpha \sin\beta(1+\gamma)\theta_{y'}]}{[\cos\alpha - \sin\alpha(1+\gamma)\theta_{x'}]^2} \tag{47}$$

$$\frac{\partial \Delta x}{\partial \theta_{y'}} = -\frac{(\gamma t + d_b)\sin\beta}{\cos\alpha - \sin\alpha(1+\gamma)\theta_{x'}} \tag{48}$$

$$\frac{\partial \Delta y}{\partial \theta_{x'}} = \frac{(\gamma t + d_b + \Delta_m)[\sin\beta + \sin\alpha\cos\beta(1+\gamma)\theta_{y'}]}{[\cos\alpha - \sin\alpha(1+\gamma)\theta_{x'}]^2} \tag{49}$$

$$\frac{\partial \Delta y}{\partial \theta_{y'}} = \frac{(\gamma t + d_b + \Delta_m)\cos\beta}{\cos\alpha - \sin\alpha(1+\gamma)\theta_{x'}}. \tag{50}$$

The expression for the Bayesian PDF has thus been completely developed, except for $f(x_{0t}, \phi_{0t})$ and $f(p_0|x_{0t}, \phi_{0t})$. These two PDFs are the priors for the initial muon position, direction and momentum. For real data, $f(p_0|x_{0t}, \phi_{0t})$ is simply the cosmic ray muon momentum spectrum as a function of the initial position and direction for the analysed events,

which can be approximated simply by the cosmic ray muon momentum spectrum averaged over all zenith angles and positions. $f(x_{0_t}, \phi_{0_t})$ is the position and direction distribution of the analysed events. Since the position resolution of the detector is much narrower than the widths of this distribution, using a flat prior in this case should not affect the estimator significantly. Only the fit parameters for the events touching edges of the detector should be sensitive to this prior, but these events are likely already affected by other edge effects.

In this section, a Bayesian estimator intended to reconstruct the momentum of muons going through the spectrometer has thus been developed in detail. The procedure to compute the Bayesian PDF is thus summarised by the following:

1. Use the current values for x_{i_t} and y_{i_t}, $i \in \{-1, 0, \ldots, n\}$ to evaluate $f(x_{i_m} - x_{i_t})$.
2. Use (x_{-1_t}, y_{-1_t}) and (x_{0_t}, y_{0_t}) to compute α_0 and β_0. They are given by

$$\alpha_0 = \arctan\left(\frac{\sqrt{(x_{0_t} - x_{-1_t})^2 + (y_{0_t} - y_{-1_t})^2}}{\Delta z_0}\right) \tag{51}$$

$$\beta_0 = \arctan(y_{0_t} - y_{-1_t}, x_{0_t} - x_{-1_t}), \tag{52}$$

   where Δz_0 is the vertical distance between measurement planes -1 and 0.
3. "Move" to the first detector layer of the spectrometer $i \leftarrow 1$.
4. Compute the prior values $f(p_0|x_{0_t}, \phi_{0_t})$ and $f(x_{0_t}, \phi_{0_t})$.
5. Compute $\theta_{x'i}(\Delta x_i, \Delta y_i, \alpha_{i-1}, \beta_{i-1})$ and $\theta_{y'_i}(\Delta x_i, \Delta y_i, \alpha_{i-1}, \beta_{i-1})$ using the analytical solution to (25) and (26) and the current values for fitted positions.
6. Compute θ_0 for layer i using (21), (22), p_{i-1} and α_{i-1}.
7. Compute $f(\theta_{x'}|\theta_0)$ and $f(\theta_{y'}|\theta_0)$.
8. Compute the Jacobian using (45) and (47) to (50), α_{i-1}, β_{i-1}, $\theta_{x'i}$, and $\theta_{y'_i}$.
9. Compute $f(x_{i_t} - x_{i-1_t}|p_{i-1}, \phi_{i-1_t})$, as given by (43), (44) and (46).
10. Compute the expected p_i value, given p_{i-1}, α_{i-1} and β_{i-1}.
11. Compute α_i and β_i using (28) to (30).
12. Move to the next detector layer ($i \leftarrow i+1$) if there is one and go back to step 5.
13. Compute (41) using all the PDF and Jacobian values that have been calculated.
14. Minus the logarithm of the Bayesian PDF (the value from the previous step) can be computed if the estimator is computed using a minimisation algorithm.

3.3 New maximum likelihood method

Another method that can potentially be used to reconstruct the muon momentum is based on the minimisation of a negative log-likelihood function. Such a method normally allows the minimisation of the variance on the extracted estimators while having a minimal bias

on the most likely values. The likelihood function for the muon momentum reconstruction by the detector is written as

$$L = f(x_{0m}, \phi_{0m}, \vec{x}_m | p_0, \vec{p}, x_{0t}, \phi_{0t}) = \int f(x_{0m}, \phi_{0m}, \vec{x}_m, \vec{x}_t | p_0, \vec{p}, x_{0t}, \phi_{0t}) dx_{1t} \ldots dx_{nt}, \quad (53)$$

using the same notation as in the previous section. Thus, $f(x_{0m}, \phi_{0m}, \vec{x}_m | p_0, \vec{p}, x_{0t}, \phi_{0t})$ gives the probability density of a sample defined by measurements $(x_{0m}, \phi_{0m}, \vec{x}_m)$, conditional on a model which is characterised by the parameters $(p_0, \vec{p}, x_{0t}, \phi_{0t})$, and has been expressed as a marginal PDF. The non-marginalised PDF can be written as

$$f(x_{0m}, \phi_{0m}, \vec{x}_m, \vec{x}_t | p_0, \vec{p}, x_{0t}, \phi_{0t}) = f(x_{0m}, \phi_{0m}, \vec{x}_m | x_{0t}, \phi_{0t}, \vec{x}_t) f(\vec{x}_t | p_0, \vec{p}, x_{0t}, \phi_{0t}), \quad (54)$$

due to the decoupling between the measured observables $(x_{0m}, \phi_{0m}, \vec{x}_m)$ and the muon momenta when the true observable values are known. Since each position measurement is considered to be independent, $f(\vec{x}_m, x_{0m}, \phi_{0m} | x_{0t}, \phi_{0t}, \vec{x}_t)$ can be rewritten as

$$\begin{aligned} f(\vec{x}_m, x_{0m}, \phi_{0m} | x_{0t}, \phi_{0t}, \vec{x}_t) &= f(x_{0m}, \phi_{0m} | x_{0t}, \phi_{0t}) \prod_{i=1}^{n} f(x_{im} | x_{it}) \\ &= f(x_{0m} - x_{0t}, \phi_{0m} - \phi_{0t}) \prod_{i=1}^{n} f(x_{im} - x_{it}). \end{aligned} \quad (55)$$

All the PDFs involved in (54) and (55) have been expressed in the previous section. Using the same approximations that were used to obtain (41), (53) simplifies to

$$\begin{aligned} L &= f(x_{-1m} - x_{-1t}) f(x_{0m} - x_{0t}) \int_{-\infty}^{\infty} f(x_{1m} - x_{1t}) f(x_{1t} - x_{0t} | p_0, \phi_{0t}) \\ &\quad \left\{ \int_{-\infty}^{\infty} f(x_{2m} - x_{2t}) f(x_{2t} - x_{1t} | p_1, \phi_{1t}) \right. \\ &\quad \left. \left\{ \ldots \left\{ \int_{-\infty}^{\infty} f(x_{nm} - x_{nt}) f(x_{nt} - x_{n-1t} | p_{n-1}, \phi_{n-1t}) dx_{nt} \right\} \ldots \right\} dx_{2t} \right\} dx_{1t} \end{aligned} \quad (56)$$

with $p_{i-1} \approx p_{i-1}(\phi_{0t}, x_{0t}, \ldots, x_{i-1t}, p_0)$ and $\phi_{it} \approx \phi_{it}(\phi_{0t}, x_{0t}, \ldots, x_{it}, p_0)$.

From (43) to (50), it can be seen that the integrand of (56) remains quite complicated, particularly due to the recursive relations (28) to (30) and the expression for the Jacobian. As there is no analytical expression for the integrals, (56) must thus be numerically integrated. Since the number of dimensions to be integrated is $2n$, a Monte Carlo integration method is the preferred approach. Such a method also has the advantage of very easily incorporating the convolutions of the PDF $f(x_{it} - x_{i-1t} | p_i, \phi_{i-1t})$ with the measurement uncertainty

PDFs, by using random values for x_{it} and y_{it}, which are distributed as $N(x_{im}, \sigma^2_{x\,\mathrm{res}})$ and $N(y_{im}, \sigma^2_{y\,\mathrm{res}})$ respectively, to perform the integration.

There are however two problems with the likelihood method. The first problem is computational, as a large number of integration points is often required to get stable estimator values, such that it can easily take several seconds to several minutes to reconstruct the momentum for a single event. The most important shortcoming of the likelihood method is unfortunately more fundamental. Effectively, in contrast with a Bayesian estimator, a likelihood estimator for this particular application cannot fit for the "true" positions, except for $i \in \{-1, 0\}$. This is due to the fact that a likelihood function, by definition, measures the likelihood of a sample, given a model, and that such a quantity would not depend on the momentum at all if the "true" positions are part of the model parameterisation. This is why the likelihood function had to be expressed as a marginal PDF in (53), but this involves convolutions around the measured positions. Such a function evaluates the effects due to the position uncertainties, but results in a biased estimator for the momentum. On average, the likelihood function biases the momentum in the negative direction, because the measured positions are more scattered than the true positions.

3.4 Kalman filter methods

Two different variants of Kalman filter methods have also been investigated to reconstruct muon momentum. The first method that was tested is the widespread extended Kalman fitter method (EKF)[5]. For this particular application, it has been found that this method fails miserably, because in the CRIPT detector, muon momentum is measured only through the scattering angles, which have expectation values of 0 for each detector layer of the spectrometer. The extended Kalman filter provides a linear approximation for non-linear problems, but such an approximation is not useful when there is no linear term between the momentum and the scattering angles.

The second filtering method that was considered is an unscented Kalman filter[6][7]. This method is known to have the potential of significantly improving results compared to the EKF method when applied to a nonlinear system. However, the unscented Kalman filter is not useful either to reconstruct muon momentum in the CRIPT spectrometer, because in addition to the particularities of the system that were mentioned above, the fact that the scattering angles do not depend on their values from the previous layers in a deterministic way causes the elements of the covariance matrix related to the momentum to remain insignificant in the filter, such that the method does not provide any sensible sensitivity to the momentum.

3.5 Bayesian estimator simulation results

To test the performance of the Bayesian estimator method, simulated events with different energies have been reconstructed using the algorithm. The parameters used for the tests are the following:

Detector plane dimensions	:	200 cm × 200 cm
Number of spectrometer layers (n):		2
Steel plate thickness (t)	:	10 cm
Position resolution ($\sigma_{x\text{res}}$, $\sigma_{y_{\text{res}}}$)	:	2 mm
d_a	:	10 cm
d_b	:	35 cm
Δ_m	:	0 cm
Δz_0	:	100 cm
Muon mass (m_μ)	:	105.658367 MeV
Radiation length of steel ($X_{0\text{Fe}}$)	:	13.84/7.874 cm

A configuration that includes 10 cm plates has been found to be optimal, due to the limited height and position resolution of the spectrometer.

Events were generated using a Monte Carlo algorithm that uses the same small angle approximations as the reconstruction algorithm, except that it does not approximate the correlation between the deviation and the scattering angles. A uniform distribution in β was used along with a PDF

$$f(\alpha) = \frac{4}{\pi}\cos^2\alpha, \quad \left(0 \leq \alpha \leq \frac{\pi}{2}\right) \tag{57}$$

for the angular distribution of the incoming muons. Muon momentum has been approximated to be constant across the detector layers for both algorithms. Analyzed events are those whose true and the measured positions for the two tracking layers and for all spectrometer layers are located within the boundaries of the detector planes. For the results shown in this section, muons were either generated using a fixed momentum, or using a continuous PDF based on the measured flux distribution[8]. For the reconstruction algorithm, the following priors were used:

$$f(x_{0_t}, \phi_{0_t}) \propto 1 \tag{58}$$

$$f(p_0|x_{0_t}, \phi_{0_t}) \propto \begin{cases} \alpha e^{\beta_1\left[\frac{p_0}{\text{MeV}}\right]^{r_1}} + e^{\beta_2\left[\frac{p_0}{\text{MeV}}\right]^{r_2}} & p_0 > 576 \text{ MeV} \\ 0 & \text{otherwise} \end{cases}, \tag{59}$$

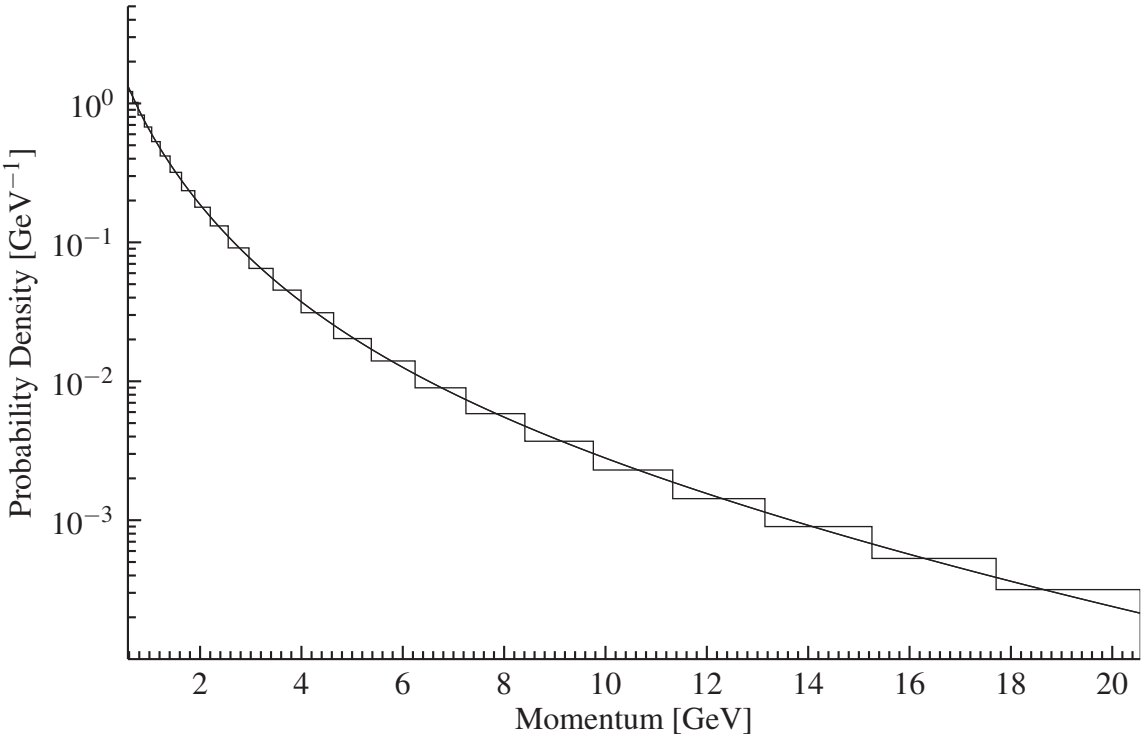

Figure 4: *Analytical function used as the momentum prior for reconstruction compared to a PDF obtained from results shown in [8].*

where

$$\alpha = 4.16748657924594035 \tag{60}$$
$$\beta_1 = -5.91500606777898147 \times 10^{-2} \tag{61}$$
$$r_1 = 5.68388489308096045 \times 10^{-1} \tag{62}$$
$$\beta_2 = -1.12723862539844066 \times 10^{-1} \tag{63}$$
$$r_2 = 4.43543354172820592 \times 10^{-1}. \tag{64}$$

Figure 4 shows a plot of this function, along with a PDF extracted from the published results cited above.

To evaluate the performance of the reconstruction algorithm, the following metrics are considered:

Relative error distribution peak bias: The relative error is computed for each reconstructed event. The distribution of the resulting values is plotted, then the location of the peak of this distribution is found. Ideally, we would like the peak to be at 0.

"1σ" confidence interval: This interval is computed by finding the relative error values that allow to include 68.269% of the successfully reconstructed events on each side of the relative error distribution peak.

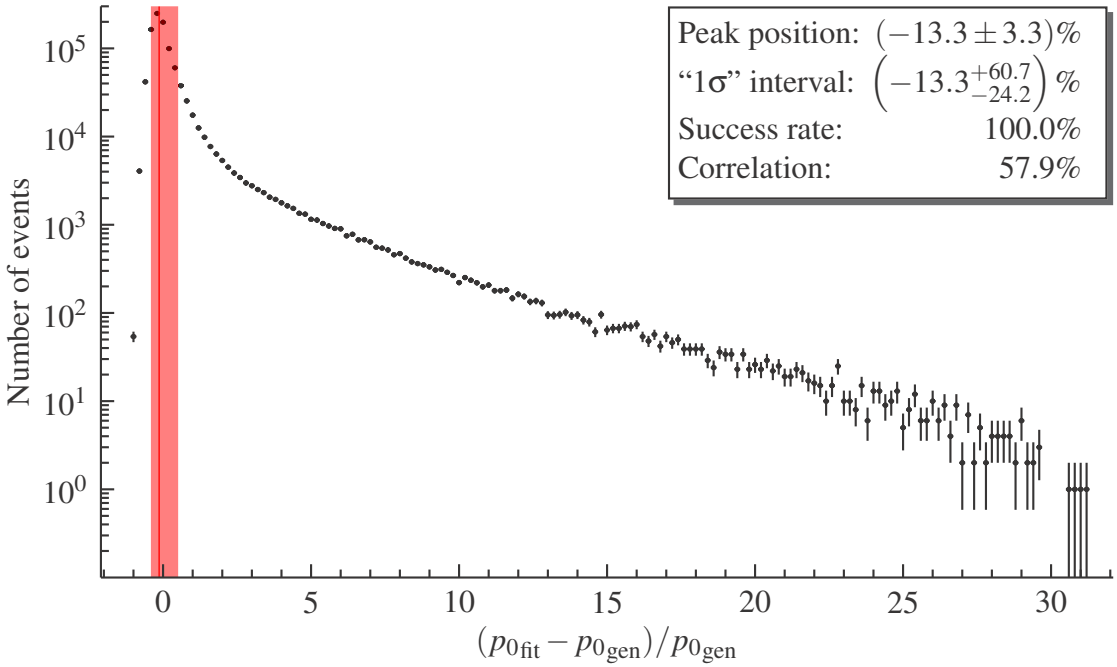

Figure 5: *Distribution of relative reconstruction error for 10^6 events generated according to the cosmic ray muon spectrum and reconstructed using a cosmic ray muon spectrum prior. The red band shows the "1σ" confidence interval.*

Correlation with true momentum: The correlation between the successfully reconstructed and the generated momentum is computed, to ensure that the reconstructed values are driven by the true values rather than being randomly distributed.

Reconstruction success rate: This is the number of successfully reconstructed events (having a reconstructed momentum value under 100 GeV) divided by the total number of generated events.

The first test that was performed consists in evaluating the overall performance of the reconstruction algorithm for events generated according to the cosmic ray muon spectrum, when using the cosmic ray muon spectrum prior. Figure 5 presents the results that were obtained with this test. It shows a perfect reconstruction success rate (thanks to the prior), a good correlation of 57.9% between the generated and reconstructed momenta, a moderate peak bias of -13.7% and a satisfying "1σ" confidence interval.

The second test is identical to the previous simulation, except that a flat prior was used for the reconstruction algorithm. Figure 6 shows the results for this test. Although the peak bias for this plot is not significantly different from the previous one, there are noticeable differences regarding the average success rate and correlation. When using the cosmic ray muon prior, the success rate is perfect, because the prior constrains the reconstructed momenta when the detector measurements do not provide any useful information. For such events, the reconstructed momentum is thus very weakly correlated to the generated

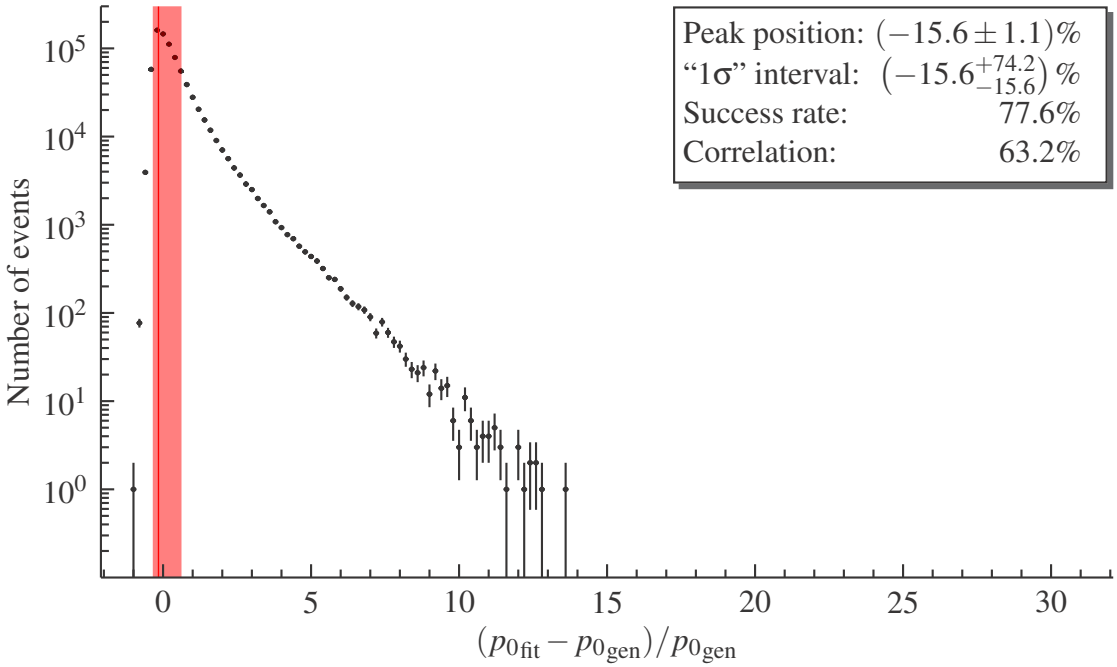

Figure 6: *Distribution of relative reconstruction error for 10^6 events generated according to the cosmic ray muon spectrum and reconstructed using a flat prior. The red band shows the "1σ" confidence interval.*

momentum, which reduces the average correlation. On the other hand, when reconstruction is performed using a flat momentum prior, events whose measured amount of scattering is negligible compared to the position resolution will see their momentum fitted to a very large, often infinite value. If one discards these events from the data, the reconstructed momentum for the remaining events is better correlated to the generated value, but this is at the cost of a lower average reconstruction success rate. This success rate depends obviously on the generated momentum. Figure 7 shows the momentum distribution for the events that fail to reconstruct.

In light of the two sets of results that have been presented so far, another possibility for the reconstruction algorithm would be to reconstruct the events using a flat prior by default, but then to fall back to a cosmic ray muon spectrum prior if the default algorithm fails. Figure 8 presents the corresponding results. It shows that the position of the relative reconstruction error distribution peak is driven by the flat prior, but the tail and the correlation are driven by the cosmic ray spectrum prior. The combined effects also tend to widen the confidence interval.

Now that the average response of the reconstruction algorithm has been assessed, it is interesting to see how this response depends on the generated muon momentum. As mentioned above, the usage of either type of momentum prior results in a similar average relative error peak bias, but we expect momentum-dependent variations. To analyse this aspect, six

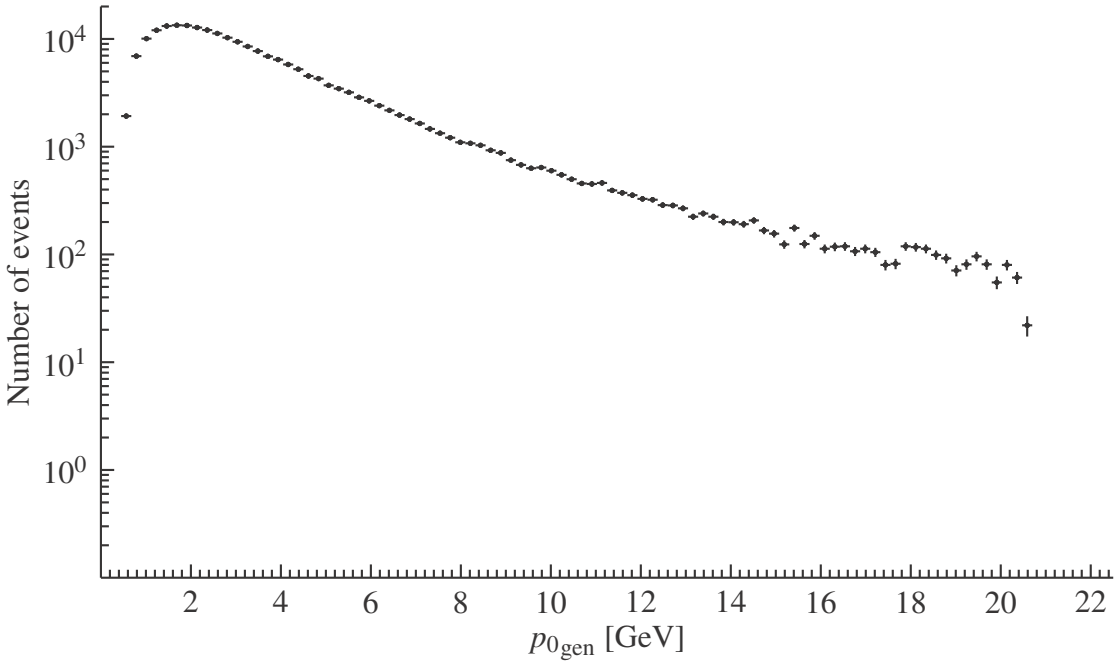

Figure 7: *Distribution of the true muon momentum for the events that fail to reconstruct in the test of Figure 6.*

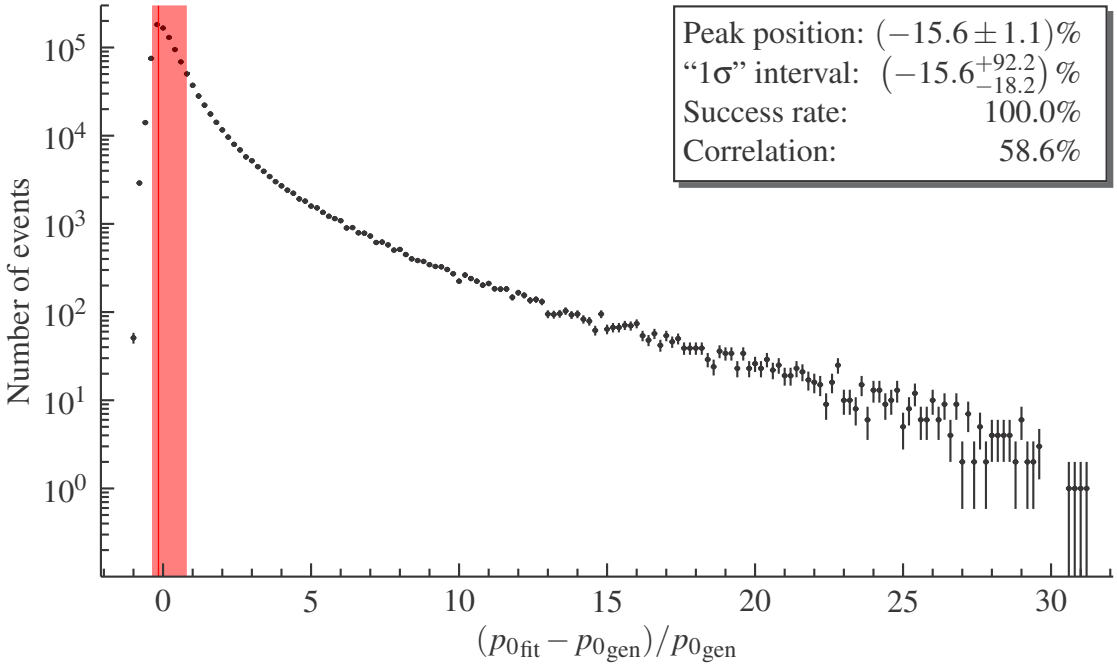

Figure 8: *Distribution of relative reconstruction error for 10^6 events generated according to the cosmic ray muon spectrum and reconstructed using a flat prior if successful and a cosmic ray muon spectrum prior if not. The red band shows the "1σ" confidence interval.*

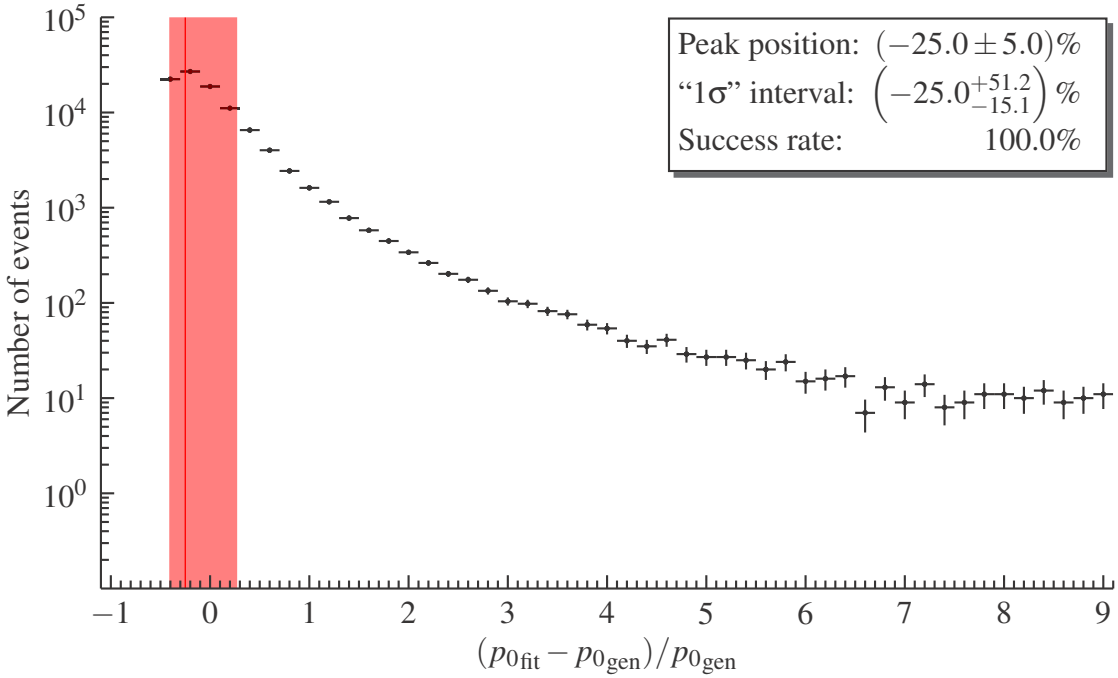

Figure 9: *Distribution of relative reconstruction error for 10^5 1000 MeV muons reconstructed using a cosmic ray muon spectrum prior. The red band shows the "1σ" confidence interval.*

different mono-energetic simulations have been generated and reconstructed using the two different priors. Figures 9 to 14 show the results obtained using the cosmic ray muon prior and Figures 15 to 20 show the corresponding results for the flat prior. As anticipated, these two sets of results are very different. The usage of the cosmic ray muon prior, although allowing to maintain a perfect success rate and narrower confidence intervals at low momentum, creates a larger peak bias for a given momentum and also a multi-peak structure for higher momenta, due to the limiting detector resolution for these events and to the fact that they are mainly constrained by the prior. This multi-peak structure is the cause of the much wider confidence intervals at higher momentum. On the other hand, a flat prior allows smaller peak biases and narrower high momentum confidence intervals, but the reconstruction success rate becomes very small for higher momenta. Table 3 summarises the results.

The last series of results that are presented in Table 4 were obtained from the same simulations as for Figures 5 and 6, but using a set of six different ranges of generated momentum. For each range, the correlation between the generated and the reconstructed momenta was computed for both the algorithm that uses the cosmic ray muon spectrum prior and the one using the flat prior. As expected, the correlation goes down significantly for both algorithms as a function of the generated momentum, but this correlation is on average significantly better when using a flat prior.

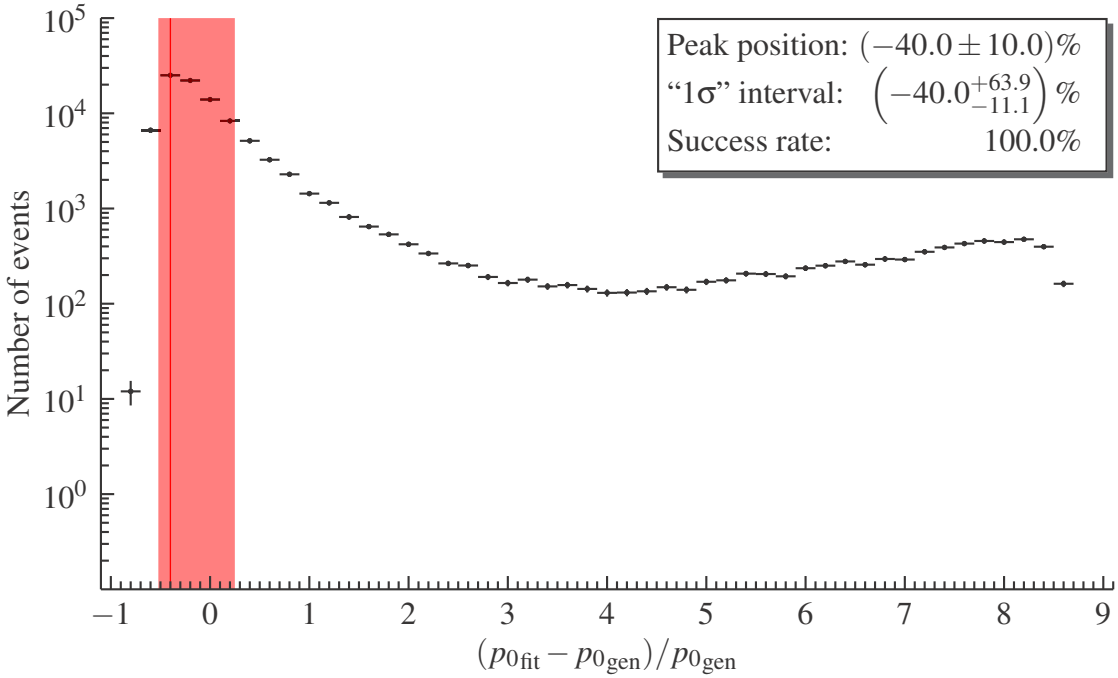

Figure 10: *Distribution of relative reconstruction error for 10^5 2000 MeV muons reconstructed using a cosmic ray muon spectrum prior. The red band shows the "1σ" confidence interval.*

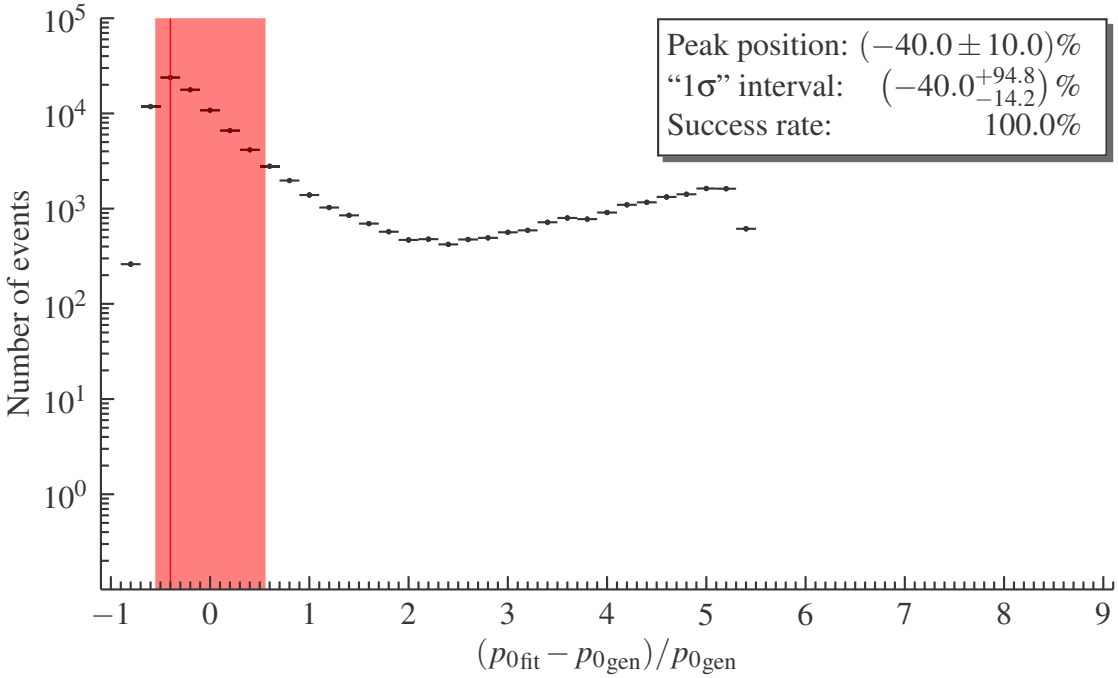

Figure 11: *Distribution of relative reconstruction error for 10^5 3000 MeV muons reconstructed using a cosmic ray muon spectrum prior. The red band shows the "1σ" confidence interval.*

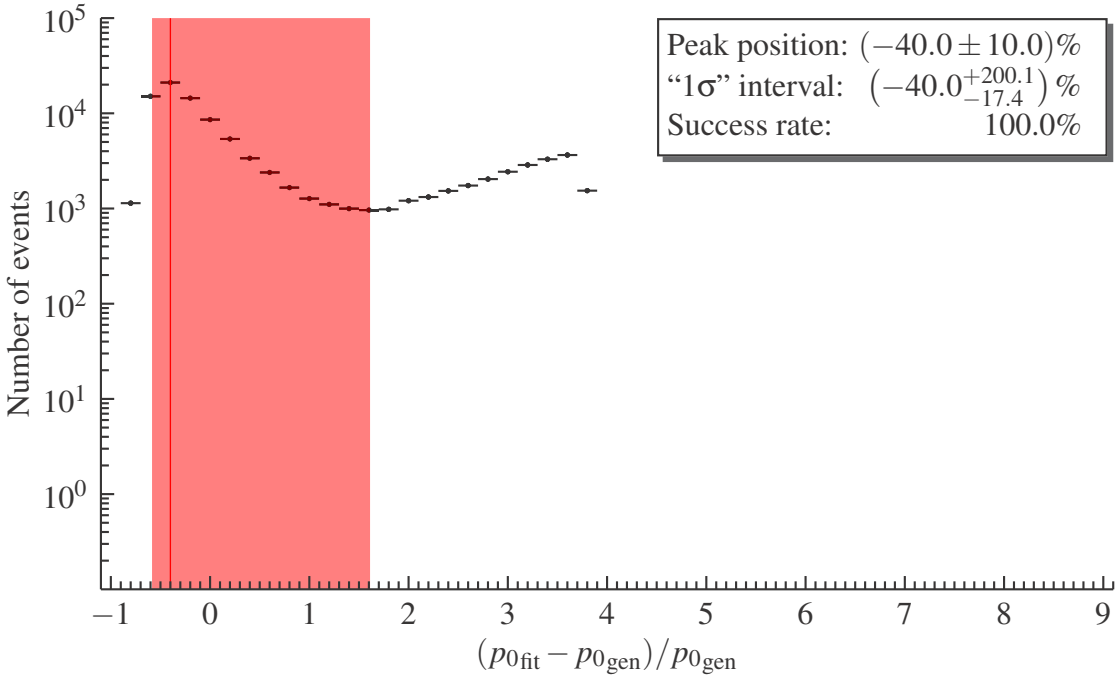

Figure 12: *Distribution of relative reconstruction error for 10^5 4000 MeV muons reconstructed using a cosmic ray muon spectrum prior. The red band shows the "1σ" confidence interval.*

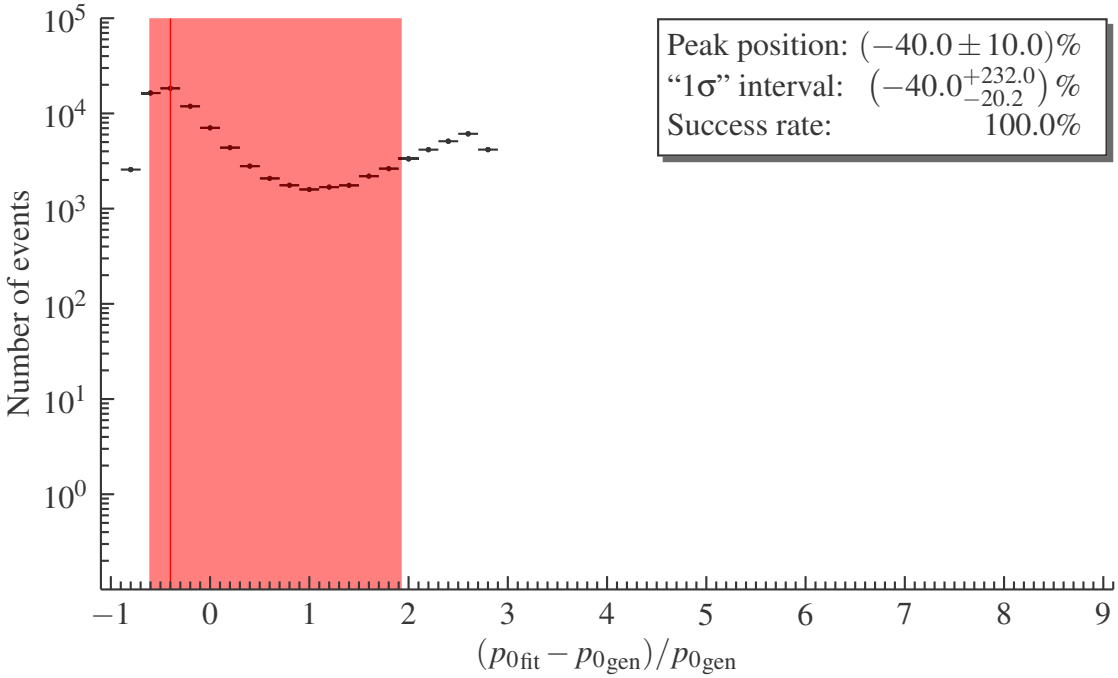

Figure 13: *Distribution of relative reconstruction error for 10^5 5000 MeV muons reconstructed using a cosmic ray muon spectrum prior. The red band shows the "1σ" confidence interval.*

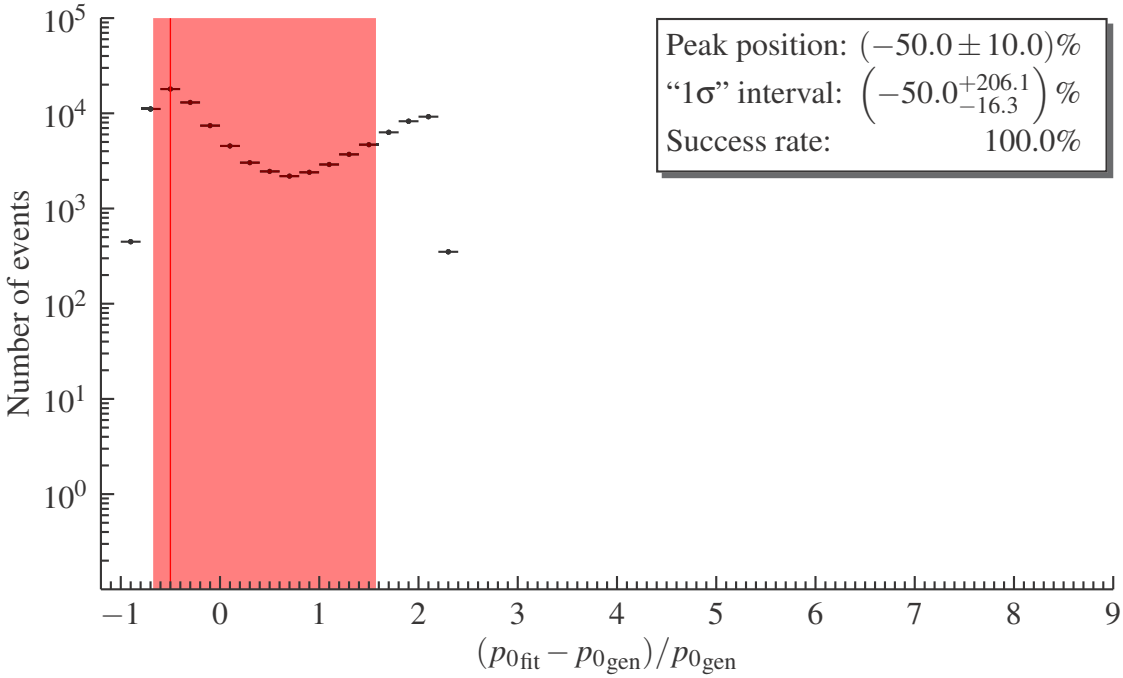

Figure 14: *Distribution of relative reconstruction error for 10^5 6000 MeV muons reconstructed using a cosmic ray muon spectrum prior. The red band shows the "1σ" confidence interval.*

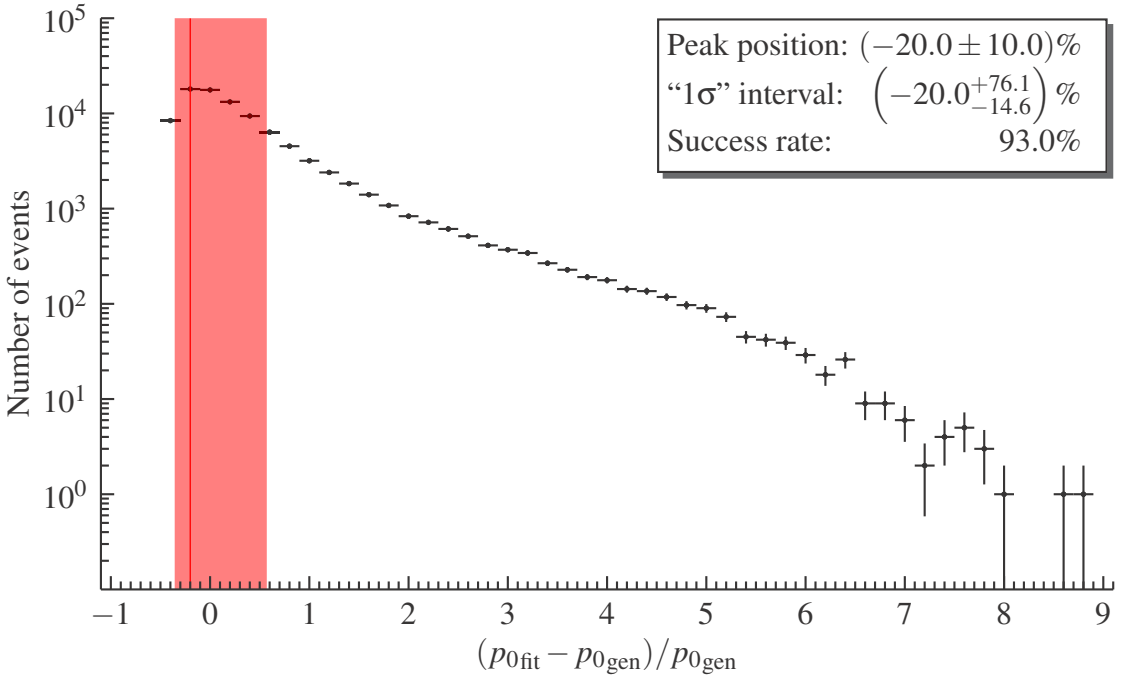

Figure 15: *Distribution of relative reconstruction error for 10^5 1000 MeV muons reconstructed using a flat prior. The red band shows the "1σ" confidence interval.*

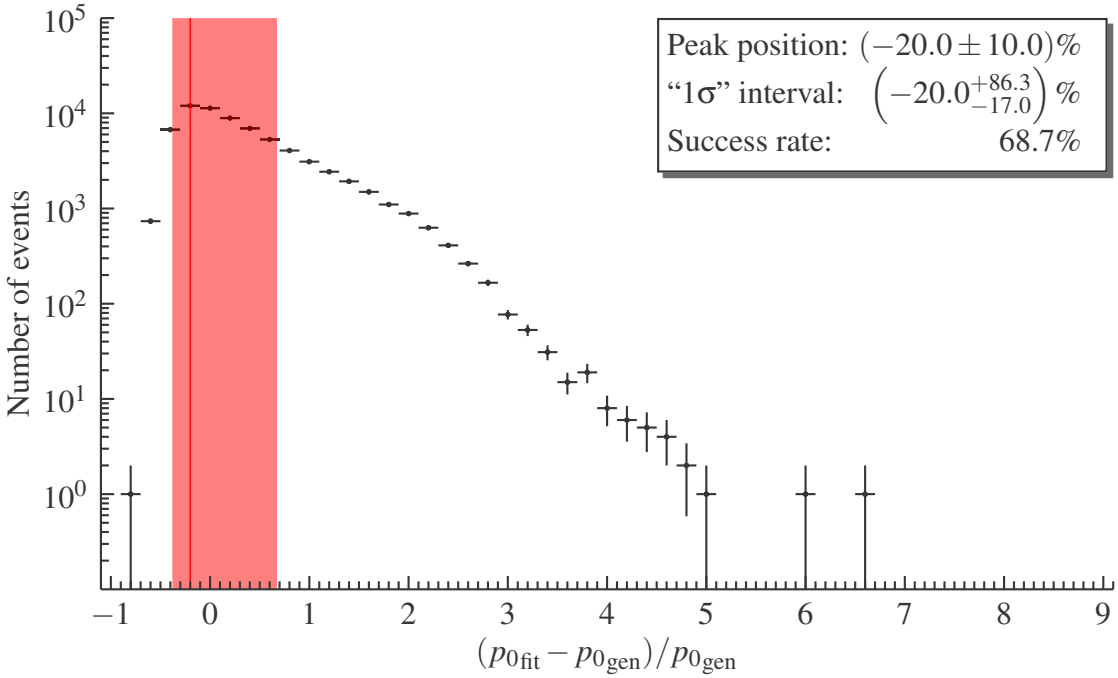

Figure 16: *Distribution of relative reconstruction error for 10^5 2000 MeV muons reconstructed using a flat prior. The red band shows the "1σ" confidence interval.*

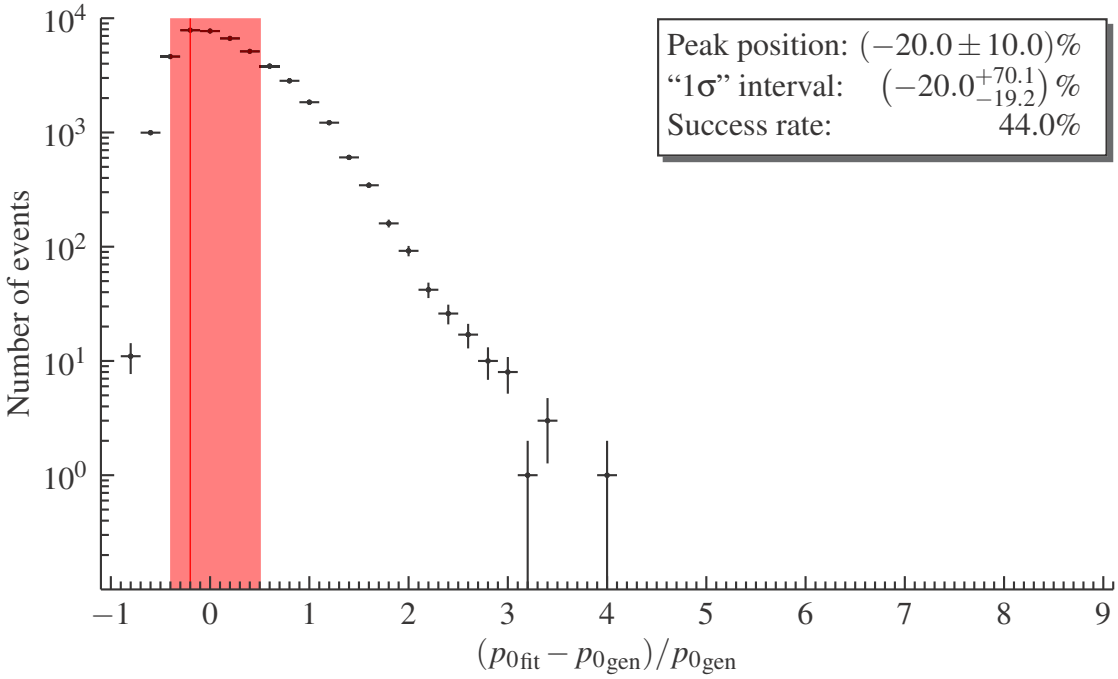

Figure 17: *Distribution of relative reconstruction error for 10^5 3000 MeV muons reconstructed using a flat prior. The red band shows the "1σ" confidence interval.*

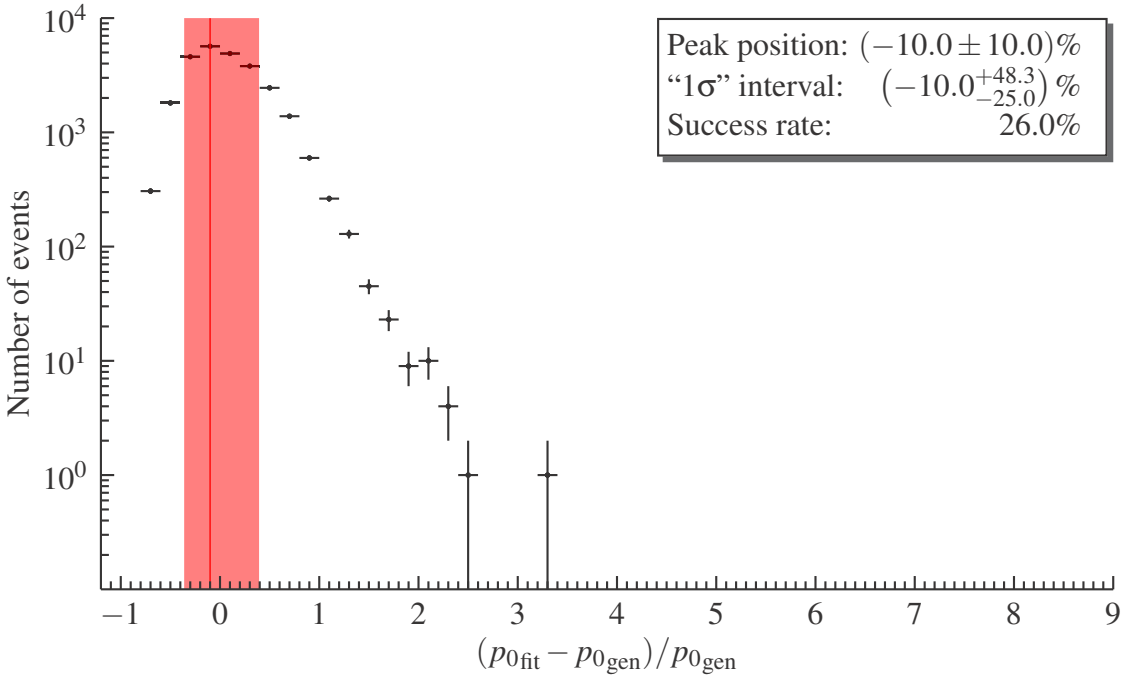

Figure 18: *Distribution of relative reconstruction error for 10^5 4000 MeV muons reconstructed using a flat prior. The red band shows the "1σ" confidence interval.*

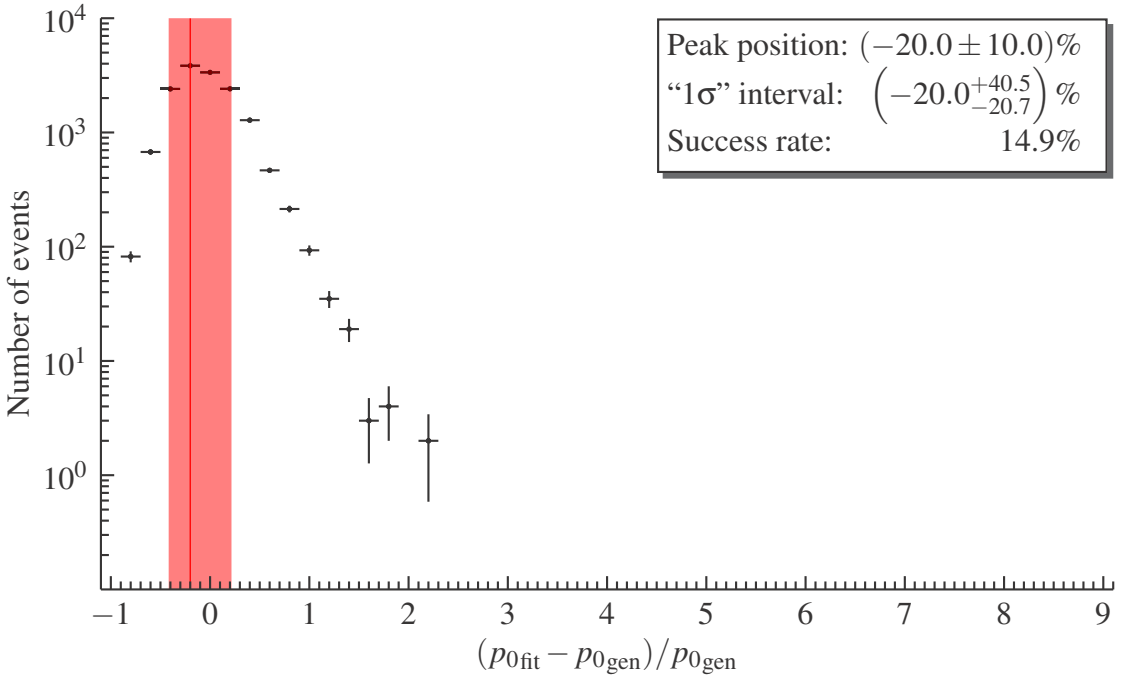

Figure 19: *Distribution of relative reconstruction error for 10^5 5000 MeV muons reconstructed using a flat prior. The red band shows the "1σ" confidence interval.*

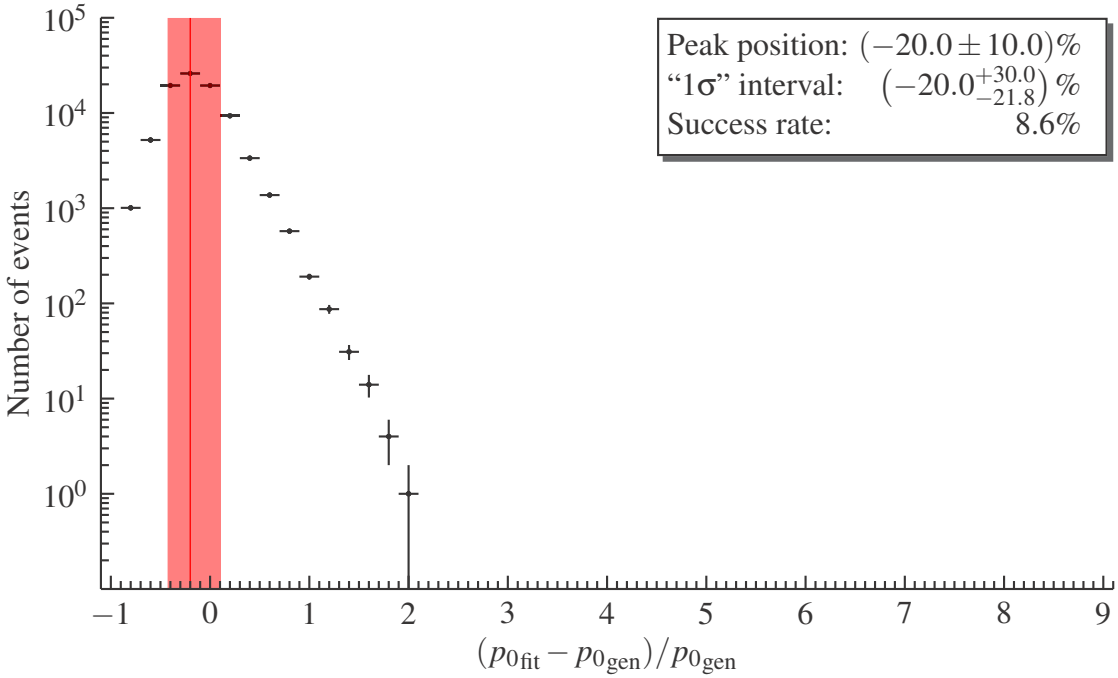

Figure 20: *Distribution of relative reconstruction error for 10^6 6000 MeV muons reconstructed using a flat prior. The red band shows the "1σ" confidence interval.*

Table 3: *Summary of the results obtained when reconstructing events generated using different momenta with the Bayesian estimator method using cosmic ray muon spectrum and flat priors.*

	Cosmic Spectrum Prior		Flat Prior	
Momentum	"1σ" Interval	Success Rate	"1σ" Interval	Success Rate
MeV	%	%	%	%
1000	$-25.0^{+51.2}_{-15.1}$	100.0	$-20.0^{+76.1}_{-14.6}$	93.0
2000	$-40.0^{+63.9}_{-11.1}$	100.0	$-20.0^{+86.3}_{-17.0}$	68.7
3000	$-40.0^{+94.8}_{-14.2}$	100.0	$-20.0^{+70.1}_{-19.2}$	44.0
4000	$-40.0^{+200.1}_{-17.4}$	100.0	$-10.0^{+48.3}_{-25.0}$	26.0
5000	$-40.0^{+232.0}_{-20.2}$	100.0	$-20.0^{+40.5}_{-20.7}$	14.9
6000	$-50.0^{+206.1}_{-16.3}$	100.0	$-20.0^{+30.0}_{-21.8}$	8.6

Table 4: *Correlation between generated and reconstructed momenta, obtained when reconstructing events generated according to the cosmic ray muon spectrum with the Bayesian estimator method using cosmic ray muon spectrum and flat priors. Results are shown as a function of the generated muon momentum range.*

Momentum Range MeV	$\mathrm{cor}(p_{0t}, p_{0f})$ Cosmic Spectrum Prior %	Flat Prior %
< 1500	22.3	41.2
$[1500, 2500[$	14.8	23.5
$[2500, 3500[$	10.2	14.1
$[3500, 4500[$	7.7	10.8
$[4500, 5500[$	5.8	8.8
≥ 5500	21.5	13.3

4 Conclusions

In this note, several muon momentum reconstruction algorithms have been presented and then evaluated. Although they are all based on the Gaussian approximation of the multiple Coulomb scattering deflection angle as a function of the incoming particle momentum, the models used by these algorithms differ through their parameterisation and the simplifications in the derivation of the minimisation function expressions.

In Section 2, a previously developed algorithm was presented. This algorithm used a likelihood function that involved a single minimisation parameter, the muon momentum, and which had a relatively simple expression, allowing very quick reconstruction time. However, since this method did not consider all correlations between the different detector layers and since it used a Gaussian approximation for the distribution of the scattering angle uncertainties due to position measurement uncertainties, the algorithm did not perform very well with large-momentum muons or the distance between layers was reduced: large biases were observed.

In order to improve muon momentum reconstruction performance, multiple other strategies were investigated. Extended and unscented Kalman filter algorithms were developed, but they both failed at providing any sensible estimator because the modelled system does not have any linear term and also due to the non-causality between the different scattering angle measurements.

An algorithm based on a more exact likelihood function was also designed. Although this solution provides some sensitivity to muon momentum, it is too computationally demanding to be practical and, more importantly, it is also susceptible to reconstruction biases. This is due to the fact that for the system to be modelled, a likelihood function does not allow, by its nature, to estimate the true muon positions, except for the two layers of the lower tracker.

Finally, a Bayesian estimator was derived, using the same minimal approximations as the new likelihood function. This estimator avoids the flaws of the new likelihood method, by having the capability of estimating the true muon positions. This improves the reconstruction time drastically, in addition to greatly reducing biases. This Bayesian estimator can behave differently, depending on the momentum and spatial distribution priors which are used for the incoming muons. Although the spatial distribution prior should not have significant effects on the results for most events, the choice of momentum prior is more important.

5 Recommendations

After analysing different muon momentum reconstruction algorithms, it is clear that the Bayesian estimator is able to reconstruct muon momentum with less bias than the other evaluated methods. It has been shown that using a cosmic ray muon momentum spectrum minimises the reconstruction success rate when events are generated using the same momentum distribution. However, the correlation between the generated and reconstructed momenta is smaller when using this type of prior because of the inclusion of events whose measured positions alone do not provide any information regarding muon momentum. For the chosen detector configuration, the fraction of events that fall within this category is about 22.4%, on average. The usage of a cosmic ray muon momentum spectrum prior thus translates into important reconstruction bias and errors, when analysed using specific muon momenta.

An alternate option for a momentum prior is the usage of a flat distribution, which does not assume any initial knowledge about the momentum distribution. This results in a lower reconstruction success rate because it excludes events whose measured positions do not provide information about their momentum. Selecting only events having a measurable momentum improves the reconstruction bias, uncertainties and correlation. The Bayesian estimator with a flat momentum prior constitutes the recommended muon momentum estimator.

References

[1] Waller, David (2010), A simulation study of the Cosmic Ray Inspection and Passive Tomography (CRIPT) muon spectrometer, (DRDC Ottawa TM 2010-168) Defence R&D Canada – Ottawa.

[2] Waller, David (2010), A simulation study of material discrimination using muon scattering tomography, (DRDC Ottawa TM 2010-211) Defence R&D Canada – Ottawa.

[3] Nakamura, K. et al (Particle Data Group) (2010), Review of Particle Physics, *J. Phys. G: Nucl. Part. Phys.*, 37(075021).

[4] Cowan, G. (1998), Statistical Data Analysis, Clarendon Press, Oxford: Oxford Science Publications.

[5] Frühwirth, R., Regler, M., Bock, R.K., Grote, H., and Notz, D. (2000), Data Analysis Techniques for High-Energy Physics, Cambridge, New York: Cambridge University Press.

[6] Julier, S., Uhlmann, J., and F. Durrant-Whyte, H. (2000), A New Method for the Nonlinear Transformations of Means and Covariances in Filters and Estimators, *IEEE Transations on Automatic Control*, 45(3).

[7] Wan, E.A. and van der Merwe, R. (2000), The Unscented Kalman Filter for Nonlinear Estimation, In *Proceedings of the IEEE 2000 Adaptive Systems for Signal Processing, Communications, and Control Symposium*.

[8] Motoki, M. et al. (2003), Precise measurements of atmospheric muon fluxes with the BESS spectrometer, *Astropart. Phys.*, 19, 113–126.

DOCUMENT CONTROL DATA

(Security classification of title, body of abstract and indexing annotation must be entered when document is classified)

1. ORIGINATOR (The name and address of the organization preparing the document. Organizations for whom the document was prepared, e.g. Centre sponsoring a contractor's report, or tasking agency, are entered in section 8.)

Defence R&D Canada – Ottawa
3701 Carling Avenue
Ottawa, ON K1A 0Z4

2. SECURITY CLASSIFICATION (Overall security classification of the document including special warning terms if applicable.)

UNCLASSIFIED
(NON-CONTROLLED GOODS)
DMC A
REVIEW: GCEC June 2010

3. TITLE (The complete document title as indicated on the title page. Its classification should be indicated by the appropriate abbreviation (S, C or U) in parentheses after the title.)

Muon momentum reconstruction algorithms for the CRIPT spectrometer

4. AUTHORS (Last name, followed by initials – ranks, titles, etc. not to be used.)

Drouin, P.-L.; Waller, D.

5. DATE OF PUBLICATION (Month and year of publication of document.)	6a. NO. OF PAGES (Total containing information. Include Annexes, Appendices, etc.)	6b. NO. OF REFS (Total cited in document.)
December 2011	46	8

7. DESCRIPTIVE NOTES (The category of the document, e.g. technical report, technical note or memorandum. If appropriate, enter the type of report, e.g. interim, progress, summary, annual or final. Give the inclusive dates when a specific reporting period is covered.)

Technical Memorandum

8. SPONSORING ACTIVITY (The name of the department project office or laboratory sponsoring the research and development – include address.)

Defence R&D Canada – Ottawa
3701 Carling Avenue, Ottawa, Ontario, Canada K1A 0Z4

9a. PROJECT NO. (The applicable research and development project number under which the document was written. Please specify whether project or grant.)	9b. GRANT OR CONTRACT NO. (If appropriate, the applicable number under which the document was written.)
30wd	

10a. ORIGINATOR'S DOCUMENT NUMBER (The official document number by which the document is identified by the originating activity. This number must be unique to this document.)	10b. OTHER DOCUMENT NO(s). (Any other numbers which may be assigned this document either by the originator or by the sponsor.)
DRDC Ottawa TM 2011-210	

11. DOCUMENT AVAILABILITY (Any limitations on further dissemination of the document, other than those imposed by security classification.)

(X) Unlimited distribution
( ) Defence departments and defence contractors; further distribution only as approved
( ) Defence departments and Canadian defence contractors; further distribution only as approved
( ) Government departments and agencies; further distribution only as approved
( ) Defence departments; further distribution only as approved
( ) Other (please specify):

12. DOCUMENT ANNOUNCEMENT (Any limitation to the bibliographic announcement of this document. This will normally correspond to the Document Availability (11). However, where further distribution (beyond the audience specified in (11)) is possible, a wider announcement audience may be selected.)

13. ABSTRACT (A brief and factual summary of the document. It may also appear elsewhere in the body of the document itself. It is highly desirable that the abstract of classified documents be unclassified. Each paragraph of the abstract shall begin with an indication of the security classification of the information in the paragraph (unless the document itself is unclassified) represented as (S), (C), (R), or (U). It is not necessary to include here abstracts in both official languages unless the text is bilingual.)

The goal of the Cosmic Ray Inspection and Passive Tomography (CRIPT) for Special Nuclear Material (SNM) Detection project is to design, build and test a large-scale muon scattering tomography (MST) system for detecting SNM and dense radiation-shielding materials like lead. Measuring the momenta of muons on an event-by-event basis is a critical part of MST as it reduces the required detection times significantly compared to making no momentum measurements. This paper describes improved algorithms for the estimation of muon momenta. Improved algorithms were required due to modifications of the CRIPT design: the spectrometer height had to be reduced from 2.0 m to 1.0 m. After investigating several momentum estimation algorithms, a Bayesian estimator, using either flat or cosmic ray muon priors, was found to be the best. These studies also resulted in a re-design of CRIPT's muon spectrometer: the number of scattering and detector layers was reduced from four to two, and the thickness of each iron scattering layer was increased from 5 cm to 10 cm.

14. KEYWORDS, DESCRIPTORS or IDENTIFIERS (Technically meaningful terms or short phrases that characterize a document and could be helpful in cataloguing the document. They should be selected so that no security classification is required. Identifiers, such as equipment model designation, trade name, military project code name, geographic location may also be included. If possible keywords should be selected from a published thesaurus. e.g. Thesaurus of Engineering and Scientific Terms (TEST) and that thesaurus identified. If it is not possible to select indexing terms which are Unclassified, the classification of each should be indicated as with the title.)

Cosmic Ray Inspection and Passive Tomography
CRIPT
Cosmic Ray Muons
Momentum Reconstruction

Defence R&D Canada

Canada's leader in Defence
and National Security
Science and Technology

R & D pour la défense Canada

Chef de file au Canada en matière
de science et de technologie pour
la défense et la sécurité nationale

www.drdc-rddc.gc.ca